NGGM
Next Generation Gravity Mission

MISSION ANALYSIS REPORT

Code : NGGM-DME-TEC-TNO-01
Issue : 1.0
Date : 30/07/2010

	Name	Function	Signature
Prepared by	Blanca Altés-Arlandis Juan Carlos Bastante Stefania Cornara Fabrizio Pirondini Matthias Renard	Project Engineer Project Manager Project Engineer Project Consultant WP Manager	
Reviewed by	Matthias Renard Stefania Cornara	WP Manager PA Manager	
Approved by	Juan Carlos Bastante	Project Manager	
Signatures and approvals on original			

DEIMOS Engenharia S.A.
Av. D.João II, Lt. 1.17, Edifício Torre Zen, 10º, 1998-023 Lisboa
Lisboa - Portugal
Tel.: +351 21 893 3010 / Fax: +351 21 896 9099
www.deimos.com.pt

This page intentionally left blank

Document Information

Contract Data	Classification
Contract Number: N/A	**Internal** ☐ **Public** ☐
Contract Issuer: Thales Alenia Space Italia	**Industry** ☑ **Confidential** ☐

Internal Distribution		
Name	Unit	Copies
Augusto Caramagno	Head of Aerospace Engineering BU	1

External Distribution		
Name	Organisation	Copies
Alberto Anselmi	TAS-I	1
Stefano Cesare	TAS-I	1

Archiving	
Word Processor:	MS Word 2007
File Name:	NGGM-DME-TEC-TNO-10.doc

Document Status Log

Issue	Change description	Date	Approved
1.0	First release version	30/07/2010	See cover page

Table of Contents

List of Figures

List of Tables

1. INTRODUCTION

1.1. Scope

The present document contains the Mission Analysis of the Next Generation Gravity Mission study.

This document is the main deliverable of the contract (NGGM/SC/DEIMOS-0981) between Thales Alenia Space Italia (TAS-I) and Deimos Engenharia (DME), under the main contract awarded by ESA to TAS-I.

This document is also compliant with the SOW of ESA ITT (reference AO/1-5914/09/NL/CT) dated November 20th, 2008 and titled "Assessment of a Next Generation Gravity Mission to monitor the variations of Earth's gravity field" [A.D.1] which is considered as fully applicable.

This version 1.0 has been prepared for MAR.

1.2. Structure of the Document

Section 2 presents theoretical considerations on Earth observation orbits, as well as a preliminary orbit selection in the 250 km – 550 km altitude range.

Section 3 introduces and studies the new ECSS-compliant atmospheric model before analysing the drag levels that the NGGM will have to cope with, depending on its orbit and on its formation-flying configuration.

Section 4 provides an analysis of the natural stability of the three FF configurations assessed at this stage of the study: In-line (in-plane), Pendulum and Cartwheel.

1.3. Acronyms and Abbreviations

AD	Applicable Document
E2ES	End-to-End Simulator
FF	Formation Flying
GNC	Guidance, Navigation and Control
GNSS	Global Navigation Satellite System
GOCE	Gravity field and steady-state Ocean Circulation Explorer
GPS	Global Positioning System
GRACE	Gravity Recovery And Climate Experiment
ITT	Invitation To Tender
LEO	Low Earth Orbit
LORF	Local Orbital Reference Frame

LTAN	Local Time at Ascending Node
LVLH	Local Vertical Local Horizontal
NGGM	Next Generation Gravity Mission
P/L	Payload
RAAN	Right Ascension of Ascending Node
RC	Repeat Cycle
RD	Reference Document
RFQ	Request for Quotation
S/C	Spacecraft
SSO	Sun-Synchronous Orbit
SST	Satellite to Satellite Tracking
TAS-I	Thales Alenia Space Italia
TBC	To Be Confirmed

1.4. Applicable and Reference Documents

1.4.1. Applicable Documents

Ref.	Document	Code	Issue	Date
[A.D.1]	"Assessment of a Next Generation Gravity Mission to monitor the variations of Earth's gravity field" Appendix 1 to AO/1-5914/09/NL/CT	EOP-SF/2008-09-1334	2	Nov 2008
[A.D.2]	"Special Conditions of Tender, Appendix 3 to AO/1-5914/09/NL/CT"	-	-	-
[A.D.3]	"Draft Contract. Appendix 2 to AO/1-5914/09/NL/CT"	-	-	Apr 2008

Table 1: Applicable Documents

1.4.2. Reference Documents

Ref.	Document	Code	Issue	Date
[R.D.1]	H.C.Euler Jr, S.W.Smith, "Future Solar Activity Estimates for Use in Prediction of Space Environmental Effects On Spacecraft", NASA, Marshall Space Flight Center, Huntsville, Alabama	-	-	Jan 2009
[R.D.2]	MSIS-E Model 1990, NASA Webpage: http://nssdc.gsfc.nasa.gov/space/model/atmos/msise.html	-	-	-

Ref.	Document	Code	Issue	Date
[R.D.3]	S. Cornara et al., "Design and Control of Formation Flying Systems for Remote Sensing Missions with Electric Propulsion", 3rd International Symposium on Formation Flying Missions and Technologies, ESA/ESTEC	-	-	Apr 2008
[R.D.4]	S. Cornara et al., "Mission Analyses and Design of Formation Flying InSAR Remote Sensing Missions with Electric Propulsion", 57th IAC, Valencia, Spain	-	-	Oct 2006
[R.D.5]	"Space Environment, European Cooperation for Space Standardization (ECSS)", ESA Publications Division, ESA-ESTEC. [ND08] of SRD.	ECSS-E-ST-10-04C	2.0	2008
[R.D.6]	B. R. Bowman, , W. K. Tobiskab, F. A. Marcos, C.Valladares "The JB2006 empirical thermospheric density model" Journal of Atmospheric and Solar-Terrestrial Physics 70 (2008) 774–793	-	-	2008

Table 2: Reference Documents

2. ORBIT ANALYSIS

2.1. Introduction

In most of Earth-observation missions, even though the processing chain elaborating the final products from the payload raw data is very complex, there is a clear correspondence between the instrument field of view (FoV) and the geolocation of the final data. Therefore, basing the mission analysis mainly on geometrical considerations, it is possible to assess the compliance of the system with coverage requirements, including spatial and temporal sampling. This allows providing the system engineer with clear recommendations in terms of orbit selection, FoV sizing and/or duty cycle optimisation.

The Next Generation Gravity Mission is more complex: the measurements are pinpoint (there is no FoV) and the elaboration of the Earth's gravity field is based on a spherical harmonics expansion. There is no direct link between the spatial or temporal sampling of the ground track at a certain point of the globe and the resolution/quality of the final data at that same point.

Therefore, this section is not aimed at performing a complete orbit selection. Section 2.2 provides general considerations about repeat orbits and sub-cycles, to be used as supporting guidelines by the scientists and the system engineers when selecting the candidate orbits to be tested with an end-to-end simulator.

For the first set of revisit performance preferences provided by the users, section 2.3 presents a preliminary orbit selection in the 250-550 km altitude range based on global orbital properties, such as repeat cycle and sub-cycles.

2.2. General Considerations on Repeat Orbits

2.2.1. Coverage Pattern

Let M be the integer number of orbits performed in one RC and Q the number of orbits per day. The Fundamental Interval S (S = 360º/Q) gives the angular space between two Ascending Node Crossings (ANX) consecutive in time. The sub-interval Si (Si = 360°/M) is the sampling angle of the Earth after an entire RC, i.e. the angle between two ANX adjacent in space. Both intervals can be expressed as angles or as distances along a certain parallel. One common way is to express them in equatorial distance (km).

Q=M/D can be written as Q=I+N/D, where I is the integer part of Q and N is an integer number. I is always greater than 16 so that the semi-major axis is greater than the Earth radius. S can therefore be written as S = D*Si. Within the Fundamental Interval S, the ANX of days n and n+1 are always separated by a distance of N or (D-N) sub-intervals Si.

A useful graphical tool to represent the relationship between spatial and temporal sampling is the Coverage Matrix. Figure 1 shows two examples. The X-axis represents the fundamental interval at the equator. The Y-axis represents the duration of an entire RC. Each square represents an ANX and shows when it occurs (number of the day written in the square, as well as ordinate) and where it falls within the Fundamental Interval (abscissa precisely represented by the vertical line). The colour of the line is based on the day and is only intended to help the reading of complex coverage matrices such as the one on the right panel.

The orbits can be classified as Drifting orbits when N=1 or N=D-1, and as Skipping orbits in the other cases. In a drifting orbit, each track falls next to the previous one, making the coverage matrix a diagonal line. The sampling of the Fundamental Interval is very progressive (see left panel of Figure 1).

Skipping orbits feature more complex coverage patterns, covering S in a more random way that reduces the persistence of large unobserved gaps (see right panel of Figure 1). However it is worth reminding that skipping orbits, which represent the large majority of repeating orbits, feature a very wide range of spatial/temporal coverage patterns.

15+16/17 SSO (Href = 284 km)	15+14/17 SSO (Href = 351 km)

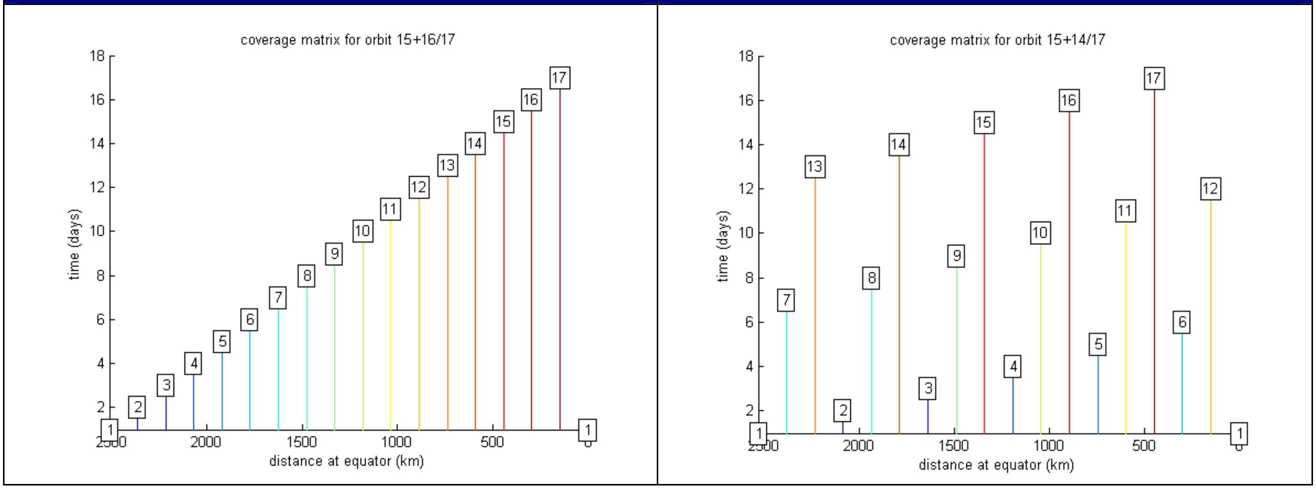

Figure 1: Coverage Matrices, Drifting (left) and Skipping (right) Orbits

2.2.2. Coverage Homogeneity

The Sub-Cycle (SC) of a repeating orbit is the smallest number of days after which an ANX falls at 1*Si or (D-1)*Si from the first ANX of day 1. The sub-cycle of a drifting orbit is obviously 1 day and the SC of the 15+14/17 SSO of Figure 1 is 6 days. This is an interesting parameter to measure how fast an orbit is in reducing the largest unobserved gap at the equator (when considering only the ascending passes).

The Sub-Cycle is computed using a simple arithmetical formula. However, with high RC orbits, it is not precise enough to assess the "homogeneity" of the coverage pattern. Some orbits do not only feature a SC but one or more pseudo Sub-Cycles that might be lower and more interesting in terms of temporal sampling. Figure 2 shows an example of a skipping orbit with a 13-day SC and a 3-day pseudo SC.

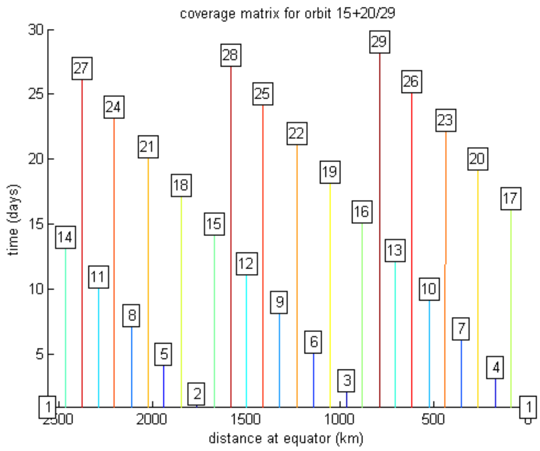

Figure 2: Coverage Matrix of the 15+20/29 SSO, Strong 3-day Pseudo Sub-Cycle

In order to better analyse the spatial/temporal sampling properties of a repeating orbit, a very interesting tool is the gap evolution graph. It consists in plotting, for each day of the RC, the width of the minimum and maximum unobserved gaps. Figure 3 shows these plots for the two orbits of Figure 1. The red curve is the equatorial width (km) of the maximum unobserved gap and the blue curve the width of the minimum unobserved gap. The black curve shows the average gap width.

Being the 15+16/17 orbit (left panel) a drifting orbit, its largest gap width is reduced as slowly as possible from S to Si and the smallest gap is immediately as wide as Si. The evolution of the gap width for the skipping orbit (right panel) is faster.

15+16/17 SSO (Href = 284 km)	15+14/17 SSO (Href = 351 km)
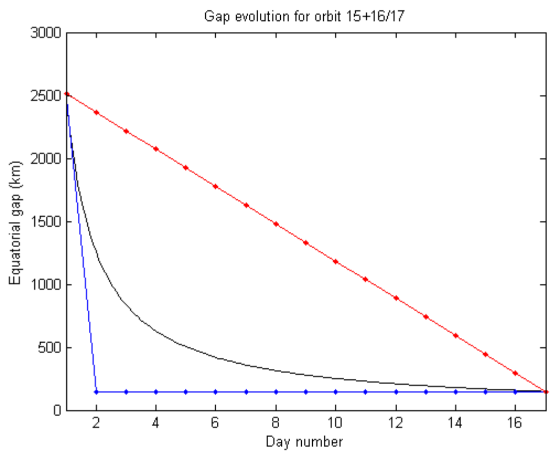	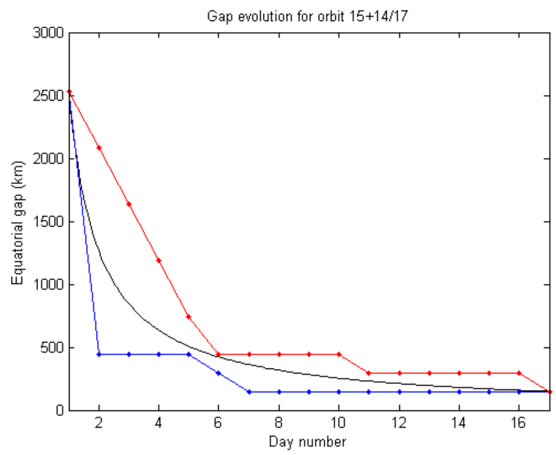

Figure 3: Gap Evolution Graphs, Drifting (left) and Skipping (right) Orbits

Sub-Cycles and pseudo SC are easy to identify on a gap evolution graph as they correspond to “waist” points where the blue and red curves get simultaneously close to the black curve. On the right panel of

Figure 3, the 6-day SC of the orbit is clearly visible. On Figure 4, the 13-day SC and the 3-day pseudo SC of the 15+20/29 Sun synchronous orbit are easily visible.

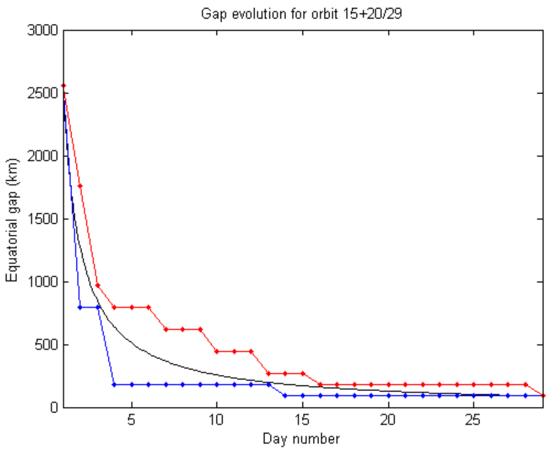

Figure 4: Gap Evolution Graph of the 15+20/29 SSO

The overall thinness of the figure drawn by the red and blue curves and the number and strength of the SC and pseudo SC are fair indicators of the homogeneity of the coverage pattern of an orbit. Figure 5 shows the coverage matrices and gap evolution graphs of three SSO featuring three different coverage profiles:

- The top panel shows plots for a drifting orbit: its coverage is progressive.
- The mid panel shows the plot for an orbit featuring an interesting strong 3-day pseudo SC, but lacking homogeneity between the 3rd and the 13th day (day of the real SC).
- The bottom panel shows graphs for an orbit featuring a very well balanced compromise between spatial and temporal sampling: on top of an 11-day Sub-Cycle, the orbit has two mild pseudo SC at 3 and 7 days that provide a very smooth evolution of the gaps width distribution with time.

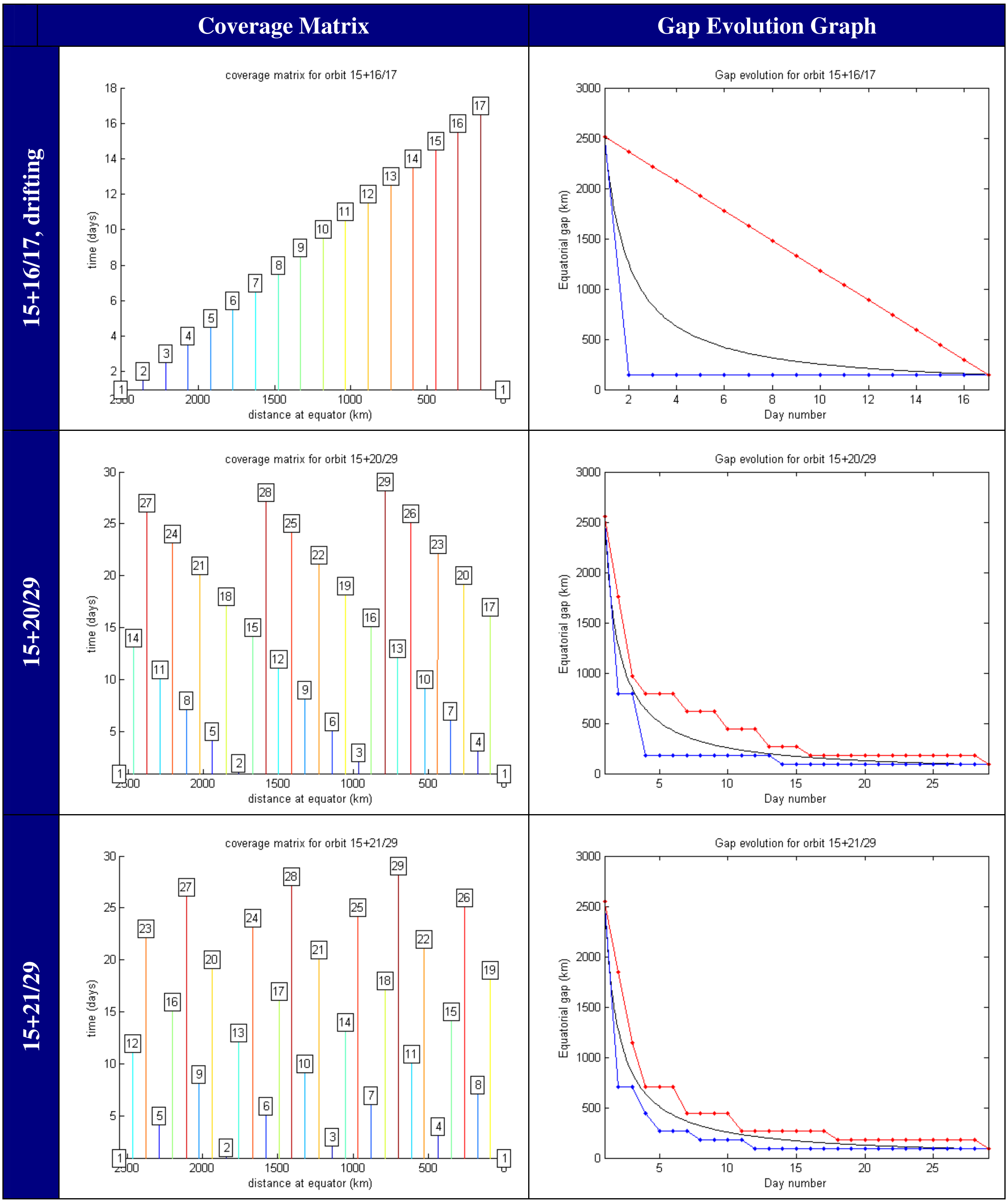

Figure 5: Comparison of the Coverage Homogeneity of 3 SSOs

2.3. Candidate Orbits between 250 km and 550 km

During the study, the users' community formulated a first set of preferences about NGGM's orbits:

- The mission may feature two pairs of spacecrafts that may fly on two different orbits
- The preferred inclination is 90°, as it provides a better resolution on the polar caps (important to study ice-related phenomena). However, two other inclinations should be studied:
  - The sun-synchronous inclination (around 97°, depending on the altitude) offers very strong advantages at system level, which can easily translate into better performance at payload level (e.g. thermal stability of the satellite-to-satellite metrology optical bench) and therefore into better scientific return as well.
  - A mid-inclination orbit may be chosen, in combination with a polar one, in order to have a better resolution at mid latitudes. The studied inclination, 62.7°, corresponds to the Bender constellation.
- The orbits should have long repeat cycles: one >30 days and the other one very long, e.g. 181 days
- The orbits should have short sub-cycles, e.g. 7 and 12 days and, if possible, an additional 4-day sub-cycle would be an asset.

The aim of this preliminary orbit selection is to look for 2 orbits between 250 km and 550 km, one with a RC>30 days (typically between 30 and 35 days) and a sub-cycle of 7 days, the other one with a RC of 181 days and a sub-cycle of 12 days. Depending on the opportunities, orbits featuring an additional 4-day sub-cycle will be preferred.

2.3.1. Orbit 1: 30d+ Repeat Cycle, 7d Sub-Cycle

Figure 6 shows the repeat sun-synchronous orbits (SSO) between 250 and 550 km (altitude on X-axis) and with a repeat cycle lower than 35 days (RC on Y-axis). The short sub-cycle is the parameter that drives the altitude selection: 6 red dots represent the 6 orbits featuring an exact 7-day RC in the altitude range of interest. An altitude area corresponds to each of them, where all the orbits have a sub-cycle of 7 days. Colour boxes show the part of these altitude ranges where the candidate orbits can be chosen. These candidates feature a 30d+ RC and a 7d sub-cycle and are represented by red dots. The colour boxes are nicely distributed between 300 and 520 km, thus providing good flexibility in terms of altitude selection.

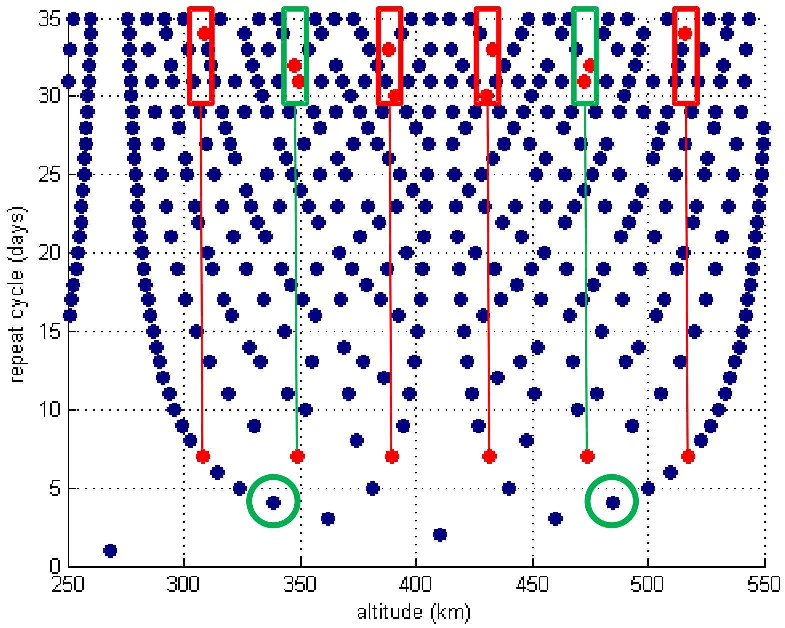

Figure 6: SSOs in the [250 km - 550 km] Altitude Range, RC ≤ 35 d

On top of that, the green circles show the two 4-day repeat orbits available in the altitude range. Being located close to them, the green boxes contain candidate orbits featuring a mild 4-day sub-cycle on top of the 7-day one. An example is given by Figure 7, showing the gap evolution of the 15+23/32 SSO (red dot at 347 km and 32 days on Figure 6). The two waist points, where the maximum gap (red curve) and the minimum gap (blue one) get close to each other, indicate the sub-cycles of the orbit: 4 and 7 days.

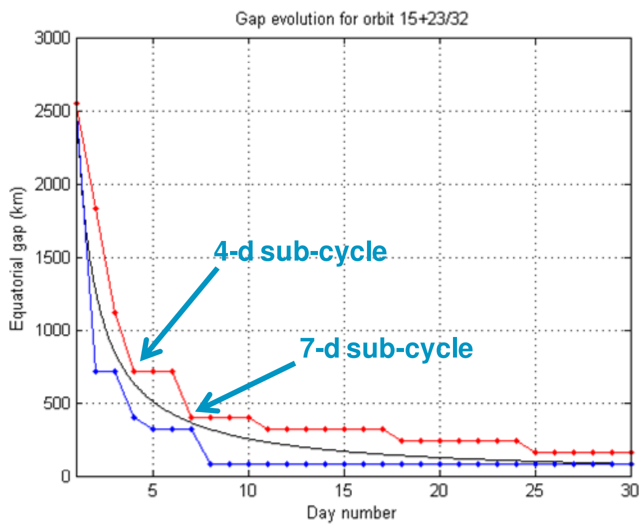

Figure 7: Gap Evolution for 15+23/32 SSO (347 km)

Figure 8 shows the same diagrams as the one on Figure 6, but for the two other studied inclinations (90° and 62.7°). The patterns and the orbit pre-selection process are exactly the same, shifted along the X-axis, i.e. in altitude.

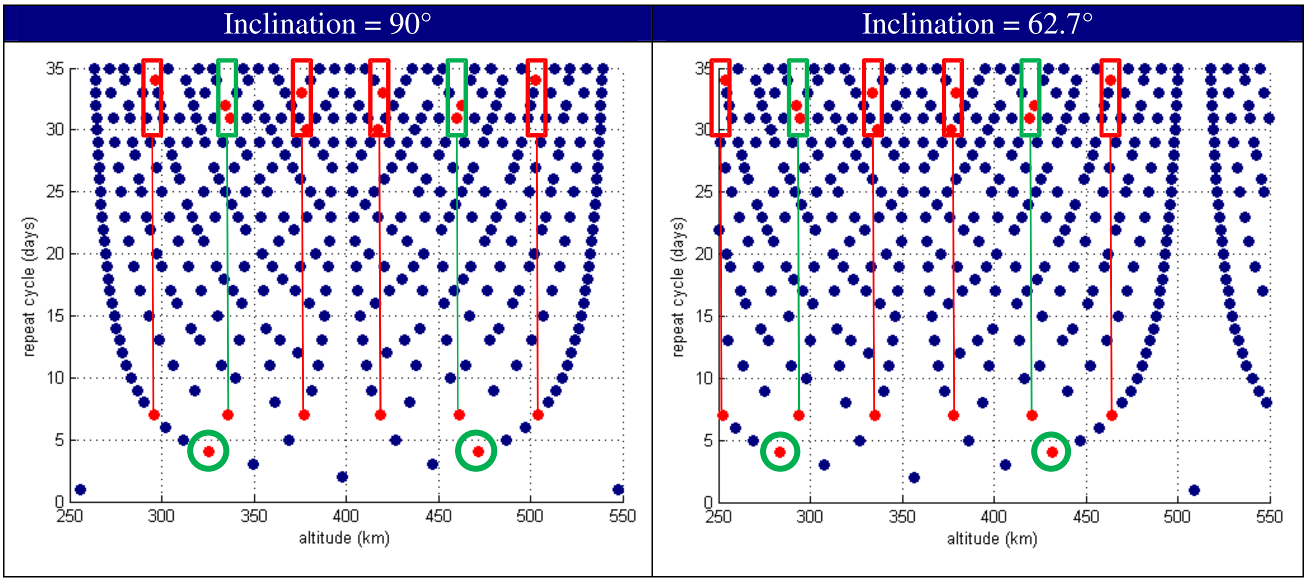

Figure 8: Polar (left) and Mid-Inclination (right) Orbits in the [250 km - 550 km] Altitude Range, RC ≤ 35 d

2.3.2. Orbit 2: 181d Repeat Cycle, 12d Sub-Cycle

Figure 9 is the same as Figure 6. The 181-day repeat orbits are not shown because they are so numerous between 250 km and 550 km that the plot would be illegible. Anyway, the selection of orbit 2 follows the same process as for orbit 1.

The 12-day sub-cycle is driving the altitude choice. However, there are only four 12-day repeat orbits in the altitude range of interest (red dots marked with arrows), thus offering only 4 altitude areas where to choose 181-day final candidates. Besides, none of them would provide a 4-day additional sub-cycle (see the green circles locating the 4-day repeat orbits) as 12 and 4 are not coprime numbers. Therefore, if the 12-day sub-cycle is a critical requirement, the candidate orbit must be close to one of the 4 available 12-day repeat orbits: at around 290, 385, 435 or 535 km.

On the other hand, if there is room for a ±1-day margin on this requirement, the blue rectangle of Figure 9 shows that there are many more altitude opportunities between 290 km and 540 km. The final candidate would then have a sub-cycle of 11, 12 or 13 days.

On top of that, the final candidate orbits located close to the 4-day repeat orbits would feature a 4-day additional sub-cycle. Figure 10 gives an example, showing the gap evolution of the 15+132/181 SSO (181-d RC and 345-km altitude). The two waist points, where the maximum gap (red curve) and the minimum gap (blue one) get close to each other, indicate the sub-cycles of the orbit: 4 and 11 days.

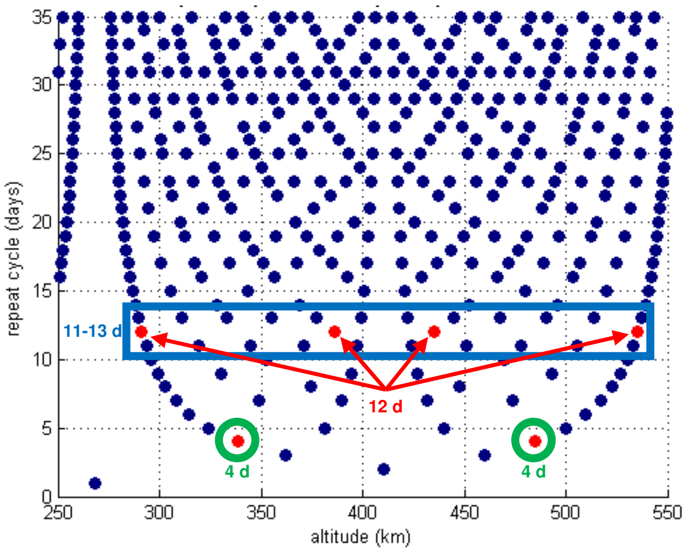

Figure 9: SSOs in the [250 km - 550 km] Altitude Range, RC ≤ 35 d

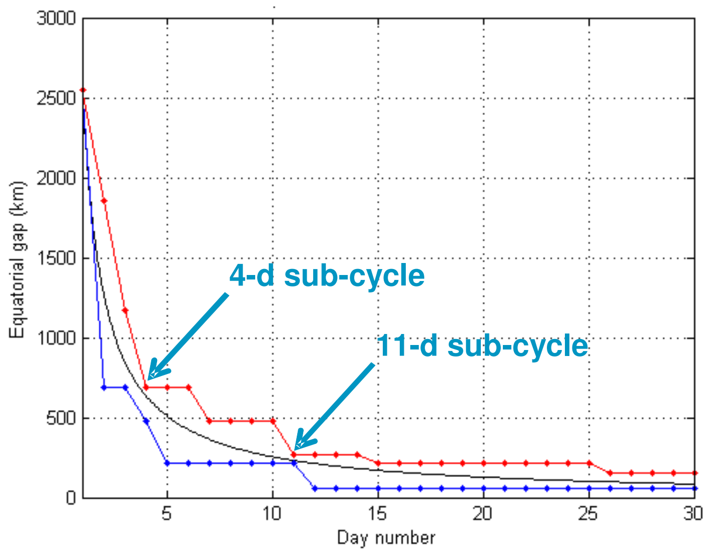

Figure 10: Gap Evolution for 15+132/181 SSO (345 km)

Figure 11 shows the same diagrams as the one on Figure 9, but for the two other studied inclinations (90° and 62.7°). The patterns and the orbit pre-selection process are exactly the same, shifted along the X-axis, i.e. in altitude.

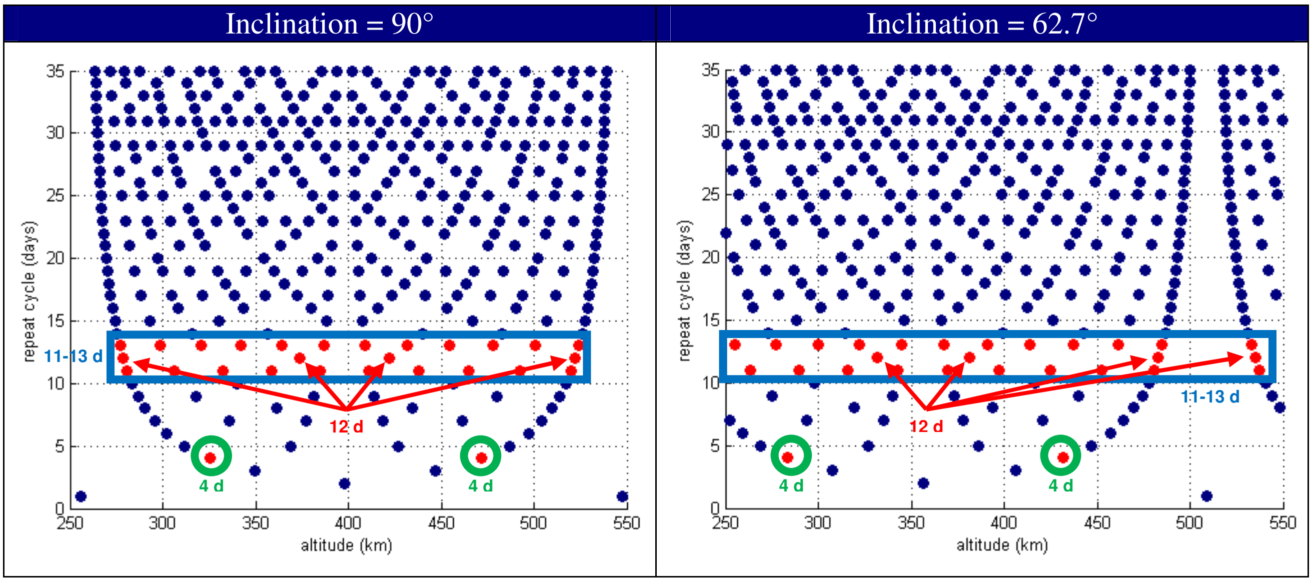

Figure 11: Polar (left) and Mid-Inclination (right) Orbits in the [250 km - 550 km] Altitude Range, RC ≤ 35 d

2.3.3. Conclusion

Due to the high number of options for the selection of the orbits of both satellite pairs, this section presents the mission-analysis-related aspects of the orbit selection in a synthetic way. Figure 12 gathers all the candidate orbits presented in section 2.3 in a single plot. Each dot represents an altitude where to choose a high-RC candidate orbit that will feature the low sub-cycle indicated on the Y-axis (as well as the inclination). The red dots represent the altitudes offering an additional 4-day sub-cycle. Orbits either with a 1-month RC (e.g. between 30 and 35 days) or with a very large one (e.g. 181 days) can be found close to all the points shown on the plot.

The altitude control margin is not defined yet. However, an important requirement is to avoid resonances lower than 30 days, i.e. to avoid letting the altitude drift away from the nominal position and fall into an orbit with a RC lower than 30 days. The distribution in altitude of such orbits is irregular; therefore some altitudes offer more margin than others. This information is provided by the blue curves of Figure 12: they indicate the width in km (see right-hand-side Y-axis) of the altitude “windows” between consecutive low-RC orbits.

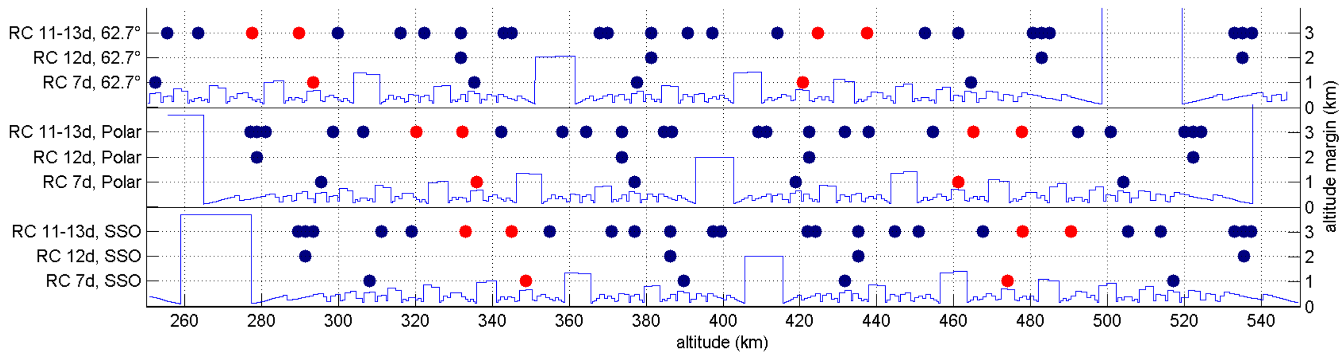

Figure 12: Orbit Pre Selection Summary

3. DRAG ANALYSIS

3.1. ECSS New Recommended Atmospheric Model: JB2006

3.1.1. Introduction

The updated Space Environment standard [R.D.5], issued in 2008 by European Cooperation for the Space Standardization (ECSS) secretariat, has introduced a new recommended atmospheric model for computing atmospheric density above 120 km. The new model, **Jacchia-Bowman 2006**, describes neutral temperature and density in the Earth's thermosphere and exosphere. It comprises a new formulation of the semi-annual density variation in the thermosphere and a new formulation of solar indexes that lead to a more accurate model representation of the mean total density.

The solar and geomagnetic activity indexes that shall be provided to the model are the following:

- F10.7: tabular value 1 day earlier plus 81-day average centred on the input time
- S10.7: tabular value 1 day earlier plus 81-day average centred on the input time
- M10.7: tabular value 5 days earlier plus 81-day average centred on the input time
- Ap: tabular value 6.7 hours earlier

The previous model, MSIS-E-90, only uses F10.7 and Ap to define, respectively, solar and geomagnetic activity. With the new model, two additional indexes are needed.

S10.7 is the solar EUV emission of the Sun and its measurements are made by SOHO satellite by means of the Solar Extreme-ultraviolet Monitor (SEM). **M10.7** is obtained from the radiation measurements of the Solar Backscatter Ultraviolet spectrometer on NOAA-16 and NOAA-17 satellites.

The guidelines provided in [R.D.5] specify that for analysis periods longer than one week and for applications that require a realistic sequence of solar activity index values for future predictions or for a specific phase of the solar activity cycle, the daily and 81-day averaged solar activity index values given in Annex 1 of [R.D.5] shall be used.

Geomagnetic activity index (Ap) monthly values are, on the contrary, not defined in [R.D.5], referring to Marshall Space Flight Center's MSAFE model [R.D.1] for geomagnetic activity index predictions.

Despite the increased accuracy of the JB-2006, the new indexes imply the use of values from cycle 23 (140-month cycle length), since no predictions are made. Besides, the Space Environment Standard does not provide monthly values for geomagnetic activity, thus obliging to use MSAFE predictions that are based on a regular 11-year (132-month) cycle model.

3.1.2. Comparison with MSIS-E-90

The differences between Jacchia-Bowman 2006 [R.D.6] and MSIS-E-90 [R.D.2] can be appreciated by comparing Figure 13 and Figure 14. These figures show the density evolution obtained in atmospheric analyses, performed with the following assumptions:

- Href = 300 km (Semi-major axis minus equatorial Earth radius)
- Polar orbit (Inclination = 89.99 degrees)
- Launch date: January 1st, 2010

- Maximum solar/geomagnetic activity conditions
- Period: full solar cycle

For the JB-2006 model (Figure 13), the maximum solar activity is defined by means of the ECSS monthly indexes for maximum activity, while geomagnetic indexes are taken from MSAFE model, with 95% of confidence (maximum activity).

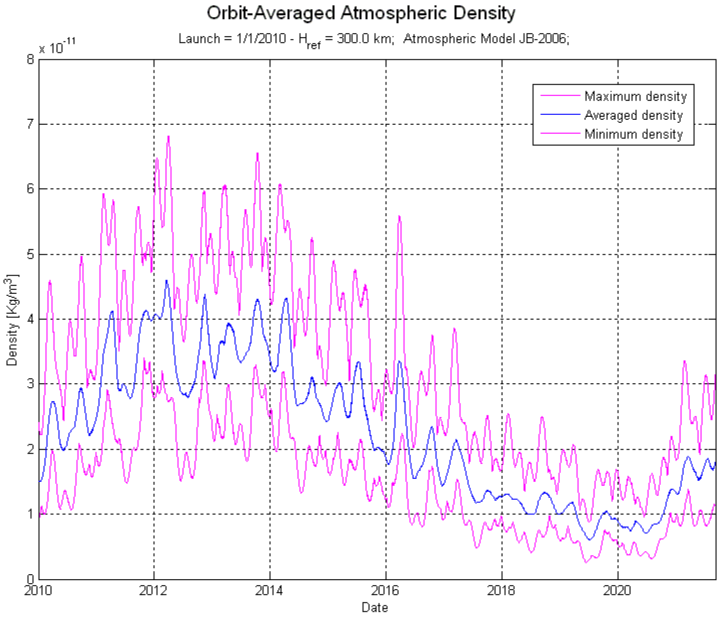

Figure 13: Atmospheric Density Evolution for a Solar Cycle with JB-2006 Model

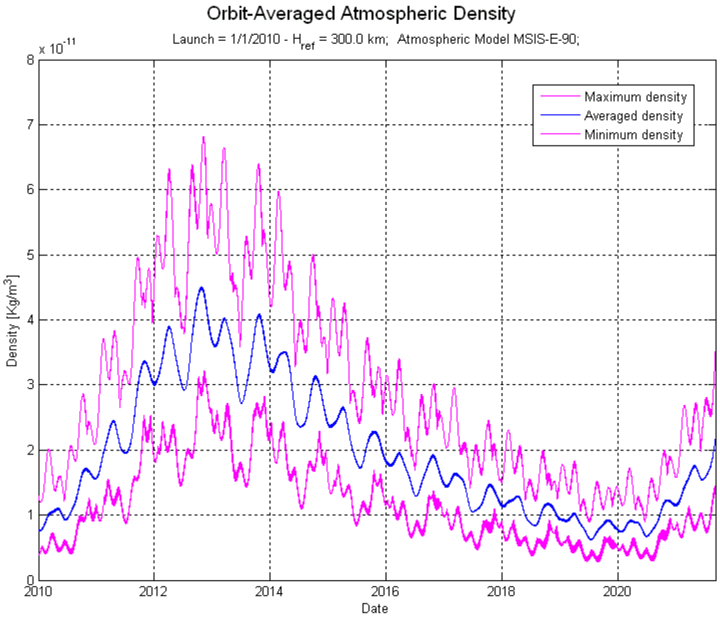

Figure 14: Atmospheric Density Evolution for a Solar Cycle with MSIS-E-90 Model

For the MSIS-E-90 analysis (Figure 14), solar and geomagnetic activity indexes are taken from the 95% confidence level of MSAFE model.

The tendency of both curves is similar, although the instantaneous differences can be quite notable. The density profiles in Figure 15 show the values for the first orbit of the complete solar cycle analyses (Figure 13 and Figure 14). On the left hand, JB2006 model returns an average density of $1.55 \cdot 10^{-11}$ kg/m^3, approximately the double of the density obtained with MSIS-E-90 for the same orbit: $0.79 \cdot 10^{-11}$ kg/m^3.

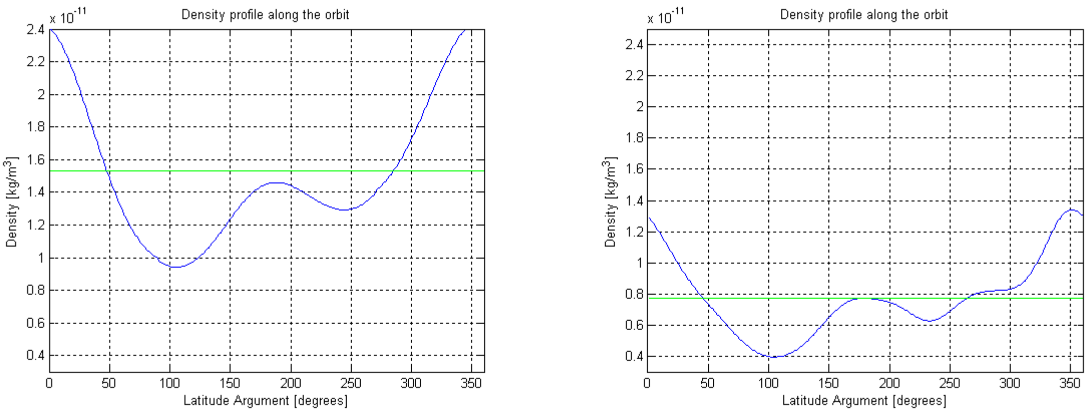

Figure 15: Density Profile along the Same Orbit for Both Models

Despite these great local divergences, the effects on long simulations are much smaller since the divergence sign alternates along the solar cycle, i.e., it is possible to find epochs where the average density obtained with MSIS-E-90 is higher than the one provided by JB2006 and vice versa.

3.2. NGGM Drag Levels over a Full Solar Cycle

3.2.1. Introduction

The atmospheric drag levels depend on the atmospheric density, which is directly dependent on the altitude. Hence, this analysis performs a parametric study, considering polar orbits with an altitude between 300 and 400 km. The results provide the maximum, mean and minimum drag force evolution for each altitude during 11 years, i.e. a complete solar cycle.

At this stage of the study, a polar orbit emerges as the most interesting choice to achieve the mission objectives and therefore all the drag analyses will be referred to it. Nevertheless, even if the results obtained for other types of orbits might be slightly different, the divergences are not as important as those caused by altitude variation.

3.2.2. Assumptions

In order to compute the required drag values, several assumptions were made:

- Altitude: from 300 km to 400 km, 20-km step
- Inclination: polar
- Launch date: 2010
- Lifetime: 11 years
- S/C mass: 500 kg
- Effective drag area of S/C body: 1 m^2 (constant)
- Drag coefficient: 2.2
- Atmospheric Model: JB-2006
- Geomagnetic Activity Conditions:
  - Case A: NASA-MSFC-MSAFE of January 2010 (maximum activity, confidence level = 95%)
  - Case B: NASA-MSFC-MSAFE of January 2010 (average activity, confidence level = 50%)
- Solar Activity Conditions:
  - Case A: ECSS(2008) indexes (maximum activity)
  - Case B: ECSS(2008) indexes (average activity)

3.2.3. Results

The results obtained for each case, are compared in terms of five different parameters. These parameters are all derived from the density-vs.-time data. They are defined and explained in the following paragraphs, with the support of one example case: 300-km altitude and maximum solar and geomagnetic activity (Case A).

Figure 16 and Figure 17 show the maximum, minimum and average density per orbit, for each orbit revolution. Figure 18 shows only the average. From these figures the five parameters are explained.

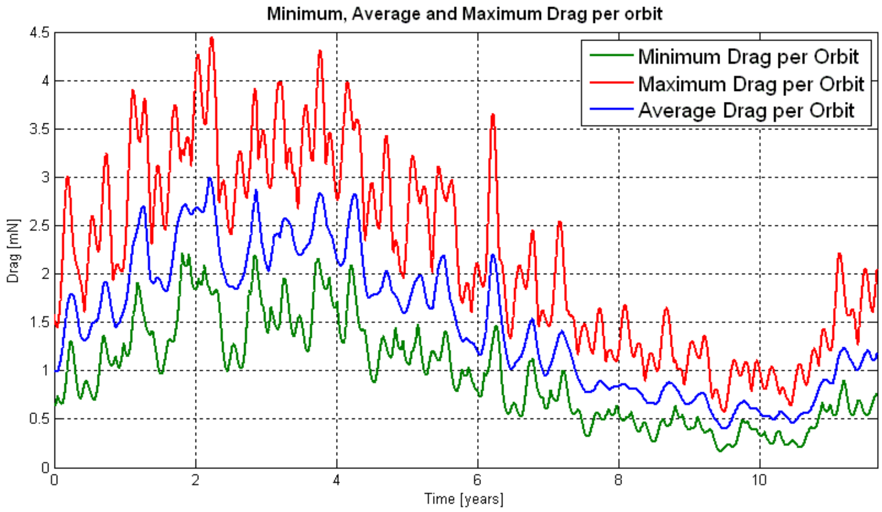

Figure 16: Drag Values Evolution for Href = 300km (I)

The first two parameters are the peak values of the complete simulations; the **Maximum drag** is the maximum value reached by the maximum drag per orbit (red line, ~4.5mN) and the **Minimum drag** is the minimum value reached by the minimum drag per orbit(green line, ~0.2mN). See Figure 17. They provide the boundary values that might appear only at some specific epoch within a complete solar cycle.

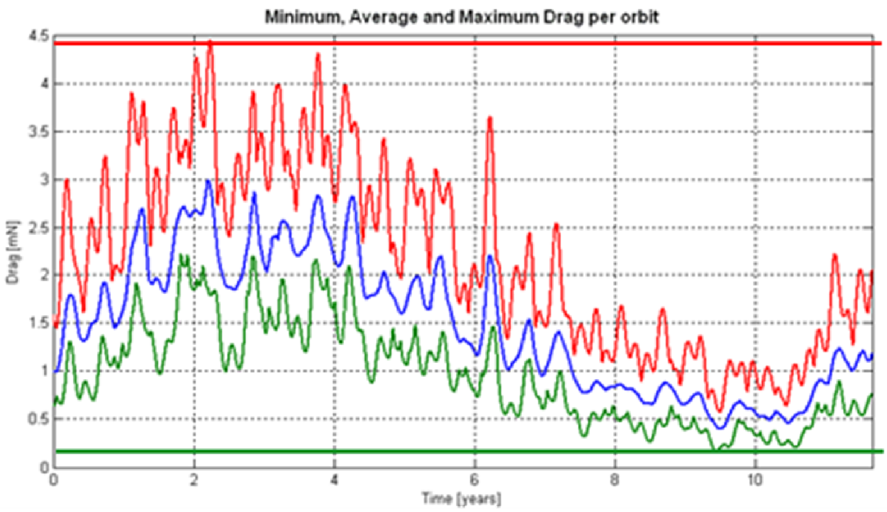

Figure 17: Drag Values Evolution for Href = 300km (II)

The other three parameters are obtained from the average drag per orbit (see Figure 18, blue line)

- **Minimum average drag per orbit** (red dashed line)
- **Mean average drag per orbit** (blue dashed line)
- **Maximum average drag per orbit** (green dashed line)

These three parameters provide a more realistic view of the drag values that should be counteracted in order to achieve drag free conditions.

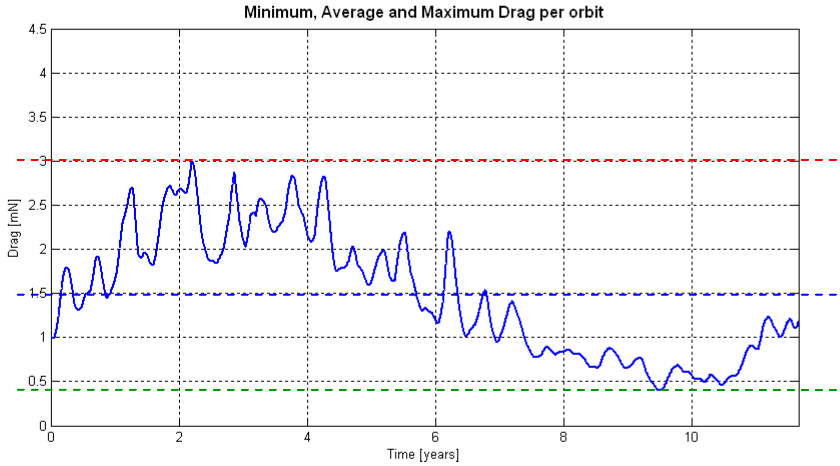

Figure 18: Drag Values Evolution for Href = 300km (III)

Considering the first case of solar/geomagnetic activity model (Case A), the drag values obtained for each altitude are shown in Table 3.

Altitude [Km]	Maximum Drag [mN]	Max.Aver. Drag [mN]	Mean Aver. Drag [mN]	Min. Aver. Drag [mN]	Minimum Drag [mN]
300	4.45	3.00	1.48	0.40	0.17
320	3.12	2.17	1.01	0.25	0.09
340	2.39	1.59	0.70	0.15	0.07
360	1.79	1.19	0.50	0.10	0.04
380	1.36	0.90	0.36	0.06	0.02
400	1.09	0.69	0.26	0.04	0.01

Table 3: Drag Force Values for Maximum Solar and Geomagnetic Activity

The analysis of the same orbits, for the Case B of solar and geomagnetic activity model, is summarised in the subsequent Table 4.

Altitude [Km]	Maximum Drag [mN]	Max.Aver. Drag [mN]	Mean Aver. Drag [mN]	Min. Aver. Drag [mN]	Minimum Drag [mN]
300	3.74	2.42	1.09	0.36	0.15
320	2.50	1.70	0.72	0.23	0.08
340	1.81	1.21	0.49	0.13	0.06
360	1.41	0.88	0.33	0.09	0.03
380	1.09	0.65	0.23	0.05	0.02
400	0.83	0.49	0.16	0.03	0.01

Table 4: Drag Force Values for Mean Solar and Geomagnetic Activity

The results of Table 3 and Table 4 highlight that the orbital altitude has larger effects on the range of drag values that shall appear along the solar cycle, than the effects of the selection between maximum or average atmospheric activity.

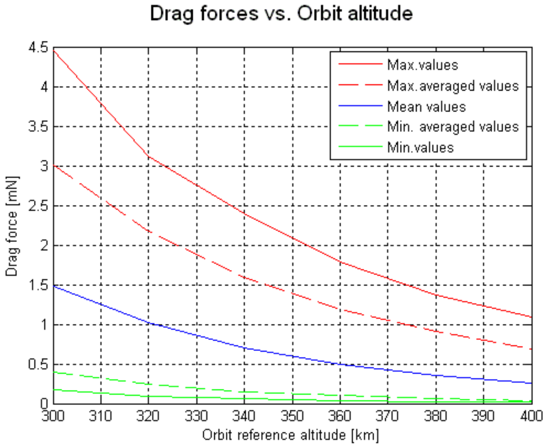

[fig.a]

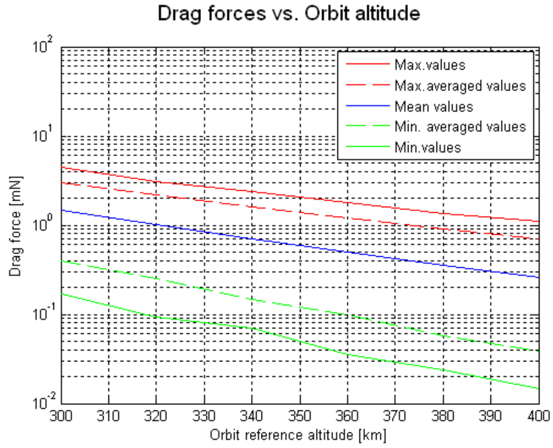

[fig.b]

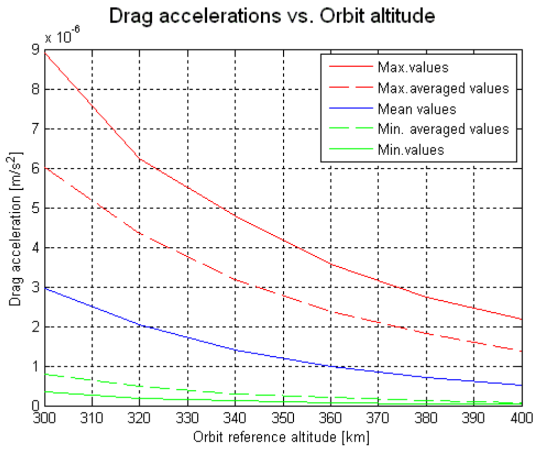

[fig.c]

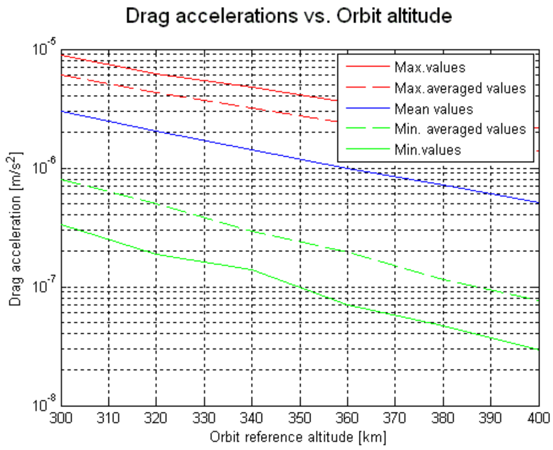

[fig.d]

Figure 19: Drag Force (top) and Acceleration (bottom) vs. Altitude in Linear (left) and Logarithmic (right) Scales, for Solar Activity Confidence Level of 95%

The graphics of Figure 19 and Figure 20 represent the evolution of drag force and acceleration vs. altitude, in linear and logarithmic scales. The 5 lines correspond to the 5 the parameters defined at the beginning of this section, expressed in drag [mN], and in acceleration [m/s^2].

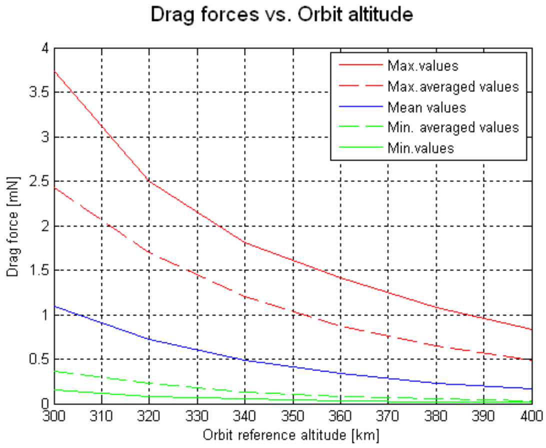

[fig.a]

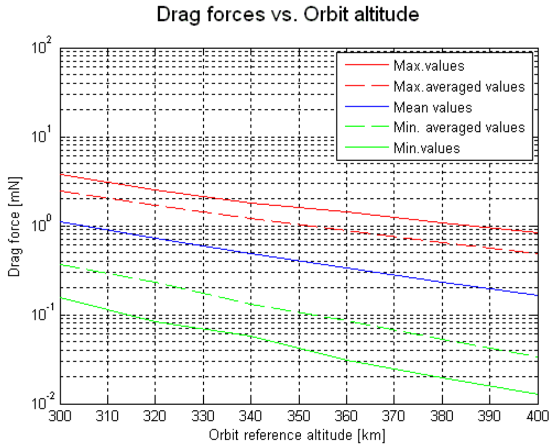

[fig.b]

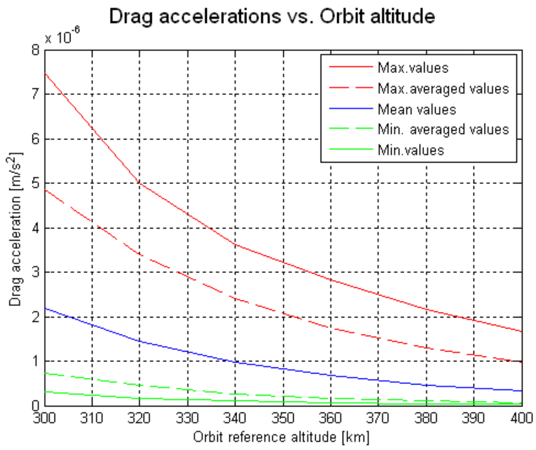

[fig.c]

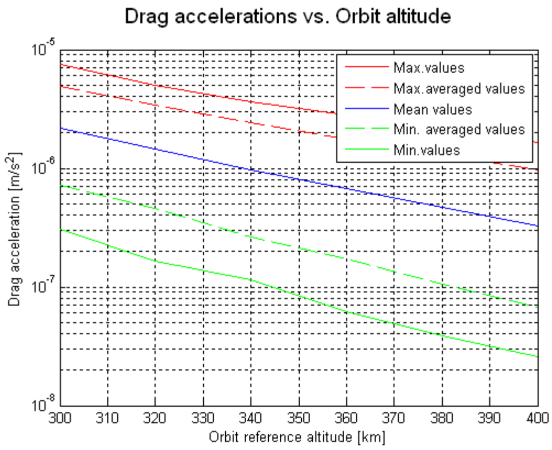

[fig.d]

Figure 20: Drag Force (top) and Acceleration (bottom) vs. Altitude in Linear (left) and Logarithmic (right) Scales, for Solar Activity Confidence Level of 50%

These graphics allow an extrapolation of the results for higher or lower altitudes by means of the logarithmic scale, since the lines almost describe a linear dependence.

3.3. Differential Drag Levels for Various Formations

3.3.1. Introduction

Each considered NGGM Formation Flying (FF) system comprises two satellites flying in different orbital configurations with a baseline (nominal inter-satellite distance) of 75 km.

In NGGM, to enable drag-free orbit conditions, the propulsion system should guarantee continuous compensation of the effect of non-gravitational forces, i.e. mainly drag, affecting each satellite independently.

These analyses provide the differential drag existing between the satellites, for each formation type, considering that both S/Cs have the same ballistic coefficient and a reference polar orbit of 350 km. Since the drag depends directly on the epoch of the solar cycle and therefore on the solar and geomagnetic activity levels as well, two epochs are chosen, representing the worst case and the best case.

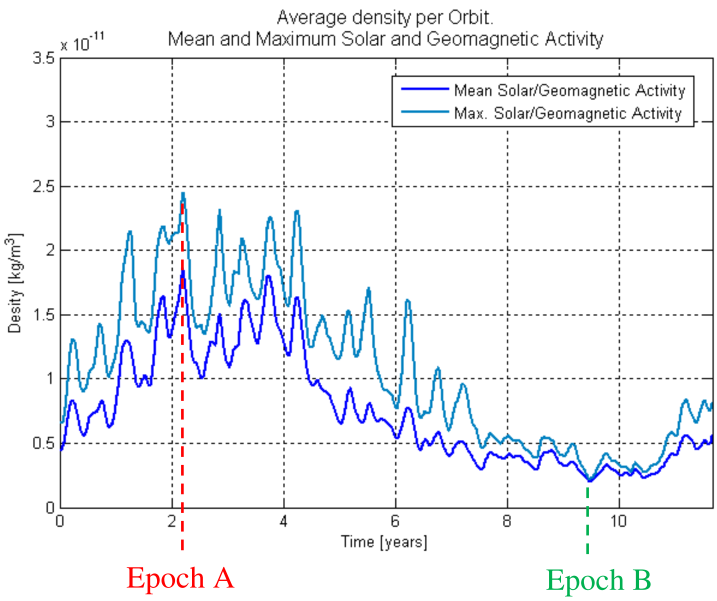

Figure 21: Epochs with Maximum and Minimum Solar and Geomagnetic Activity

Figure 21 shows the average density per orbit for two atmospheric scenarios. Starting in January 2010, the data provides values till 2021 for the maximum solar and geomagnetic activity (MSAFE 95% and Maximum ECSS values) and for the mean solar and geomagnetic activity (MSAFE 50% and Mean ECSS values)

Epoch A is defined by the date with the highest average density per orbit, when the maximum solar and geomagnetic activity levels are considered. Epoch B is, on the contrary, defined by de date with the lowest average density per orbit, when the average solar and geomagnetic activity levels are considered.

Three possible formation configurations have been taken into account:

- In-line
- Cartwheel
- Pendulum

The results of these analyses provide differential drag levels for each FF topology, and the range of possible values depending on the atmospheric activity.

3.3.2. In-Line

The in-line (in-plane) formation is an orbital system of two satellites that follow the same circular polar orbit. The altitude and mean satellite separation are respectively 350km and 75km, as described in section 3.3.1.

In this FF configuration, arranged in the reference circular polar orbit, the reference satellite separation corresponds to an Earth central angle (θ) of 0.639º (i.e. mean anomaly difference) and an in-orbit separation of ~9.8 seconds between the two spacecrafts.

In the in-line, in-plane formation, both leader and follower satellites are placed in the same orbital plane, with a given separation in mean anomaly. An alternative topology is an in-track formation, where leader and follower satellites are placed in different orbital planes and follow the same ground track. Both S/C also ideally undergo the same gravity acceleration profile, which may be beneficial for FF maintenance thanks to the minimisation of the relative drift or even for the scientific objectives of the mission.

Figure 23 provides an overview of the in-line formation geometry envisaged for the NGGM, where satellite S1 flies in the same orbit as satellite S2, approximately 9.8 seconds behind it.

This FF topology is very similar to the 2-satellite coplanar formation of the GRACE (Gravity Recovery and Climate Experiment) mission.

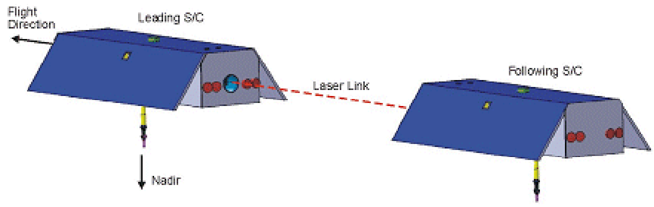

Figure 22: In-Line FF Configuration for NGGM

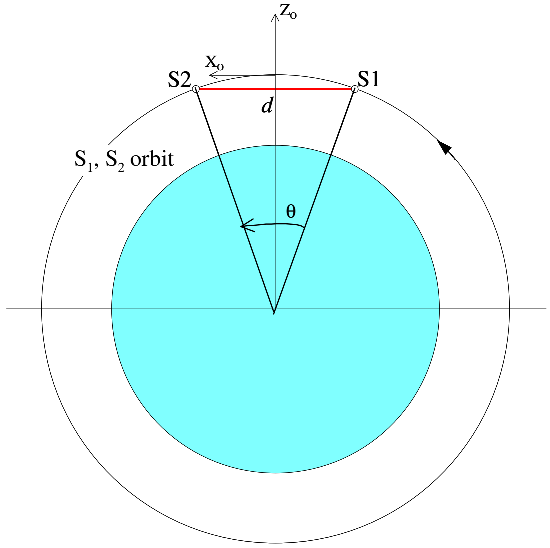

Figure 23: In-Line Formation Geometry

3.3.2.1. Results for Maximum Solar and Geomagnetic Activity

In-line drag profile over one orbit with the maximum solar and geomagnetic activity corresponds to epoch A of Figure 21. Since only a difference in mean anomaly is needed for the formation, the drag acting on each satellite is almost equal.

For this atmospheric scenario the range of variation along the complete orbit is [1.0 – 2.1] mN (Figure 24), while the maximum differential drag is about 0.007 mN.

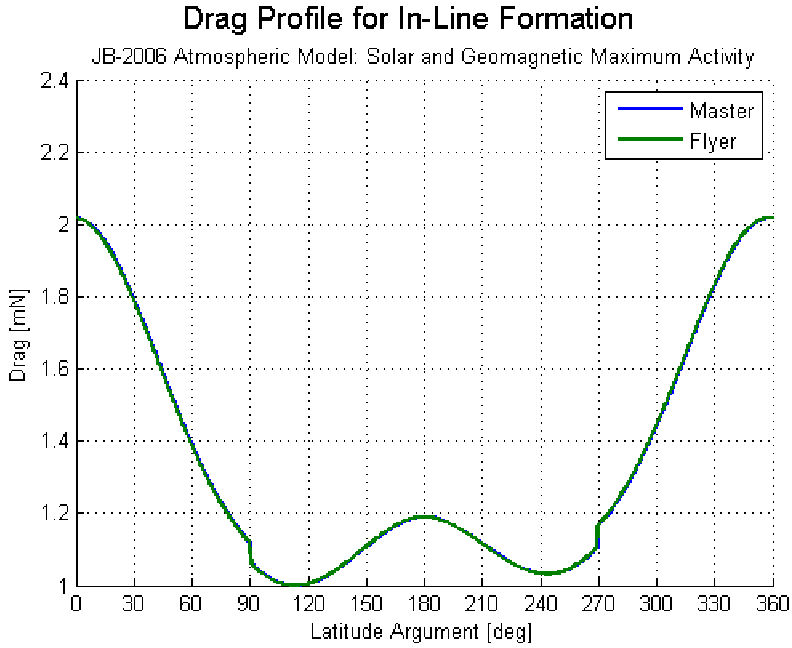

Figure 24: Differential Drag for In-line Formation. Maximum Solar-Geomagnetic Activity

The discontinuity over the poles (Figure 24, Latitude Argument = 90°, 270º) is caused by an irregularity of the JB-2006 model at the poles. The magnitude of the discontinuity depends on the direction, in which the spacecrafts cross over the poles.

Figure 25 provides a view of the JB-2006 density over the Earth, with a specifically restrained colour scale in order to highlight the density variation over the poles. The zoomed view of the North Pole shown on the right panel highlights the possible discontinuities that might appear over this zone.

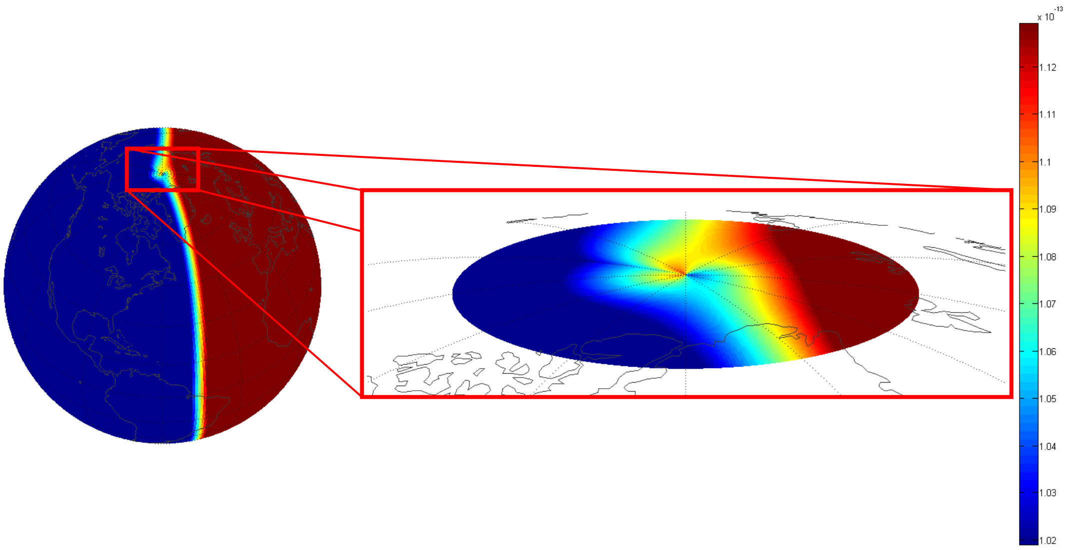

Figure 25: JB-2006 Density Discontinuity over the Poles. General View (left), North Pole Zoom (right)

3.3.2.2. Results for Mean Solar and Geomagnetic Activity

In-line drag profile over one orbit with the mean solar and geomagnetic activity corresponds to epoch B of Figure 21. As in the previous section, the differential drag is barely noticeable, since the only difference between the orbits is the mean anomaly.

The second atmospheric scenario yields to a range of variation along the complete orbit of [0.06 – 0.17] mN (Figure 26), with a maximum differential drag about 0.001 mN.

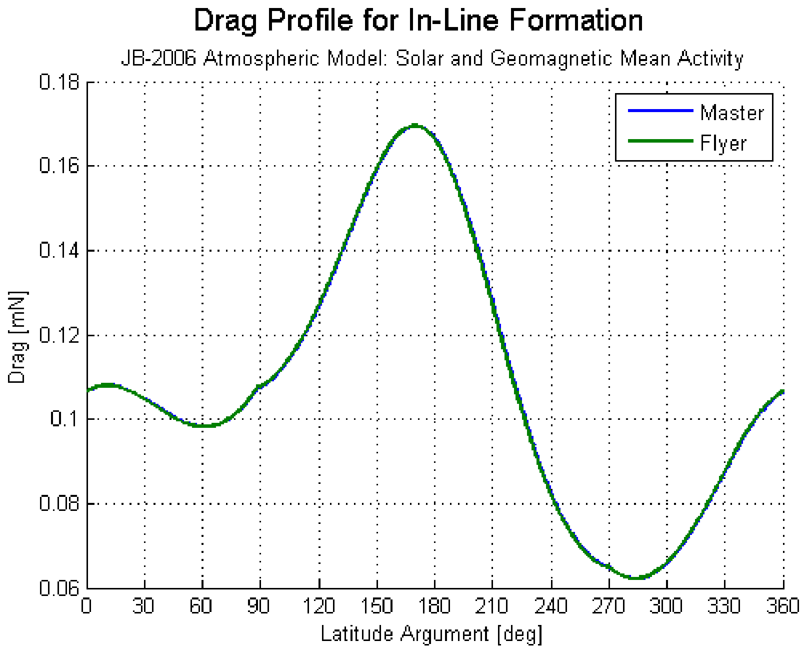

Figure 26: Differential Drag for In-line Formation. Mean Solar-Geomagnetic Activity

3.3.3. Pendulum

A **Pendulum formation** yields a cross-track (out-of-plane) relative satellite motion. This FF topology can be obtained by applying the following deltas in Keplerian elements with respect to the reference orbit of the formation ([R.D.3]):

- Deltas in inclination and/or RAAN are applied to obtain the required cross-track S/C motion. In particular, inclination deltas imply relative drift of the S/C orbital planes due to the J2 term of the Earth gravity field, while deltas in RAAN imply different effect of tesseral harmonics in both satellites and hence, also a relative drift.
- In-plane deltas may be applied on the argument of perigee and/or the mean anomalies in order to avoid collision risks at the planes crossings.

Figure 27 shows a Pendulum formation for the NGGM with two satellites along a circular polar orbit at 350 km altitude with a Δi of 0.529º between them so as to achieve a mean satellite-to-satellite distance (d) of 75 km. To avoid S/C collision when crossing the orbit nodes, the two satellites must be separated in mean anomalies, so that node passes occur at different times. An alternative consists in imposing a delta also in the RAAN of the two satellite orbital planes, so that the plane nodes do not coincide anymore. However the deltas used for node passes separation are smaller than those needed to achieve the mean distance of 75 km, and therefore they do not have relevant effects on differential drag.

In this particular Pendulum FF, with a polar orbit, the differential RAAN drift due to the J2 term of the Earth gravity field is 0.0763º/day, which yields approximately 2.3º of RAAN separation in one month.

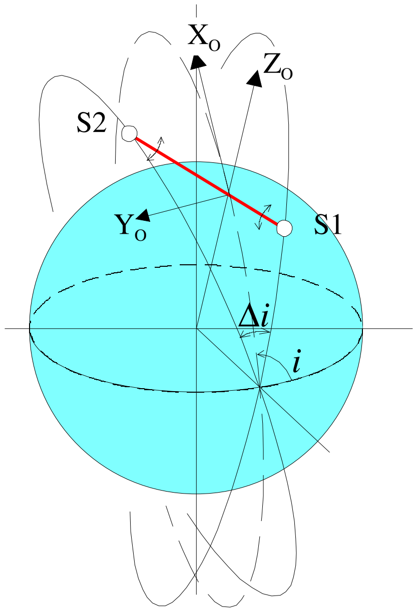

Figure 27: Pendulum Formation Geometry for Delta Inclination

There is an alternative Pendulum formation configuration based on a delta in RAAN. The delta needed to achieve a mean satellite-to-satellite distance of 75 km, in a polar orbit of 350 km of altitude, is 0.529º.

The results of the differential drag levels do not change significantly from the first pendulum configuration to the second one, therefore sections 3.3.3.1 and 3.3.3.2 only contain the results for the configuration based on a delta in RAAN. For the other case the same drag range and maximum differential drag can be assumed.

On the contrary, the formation stability analyses performed for both cases (section 4.3) will show that the formation degradation is completely different. The node differential drift due to delta in inclination results to have much greater influence than the delta in RAAN.

3.3.3.1. Results for Maximum Solar and Geomagnetic Activity

Pendulum drag profile over one orbit with the maximum solar and geomagnetic activity corresponds to epoch A of Figure 21. Since only a difference in RAAN or inclination is needed for the formation, the drag acting on each satellite is almost equal. As long as the altitudes of both satellites are the same, or almost the same, the differential drag will be very small.

For this atmospheric scenario the range of variation along the complete orbit is [1.0 – 2.1] mN (Figure 28), while the maximum differential drag is about 0.009 mN.

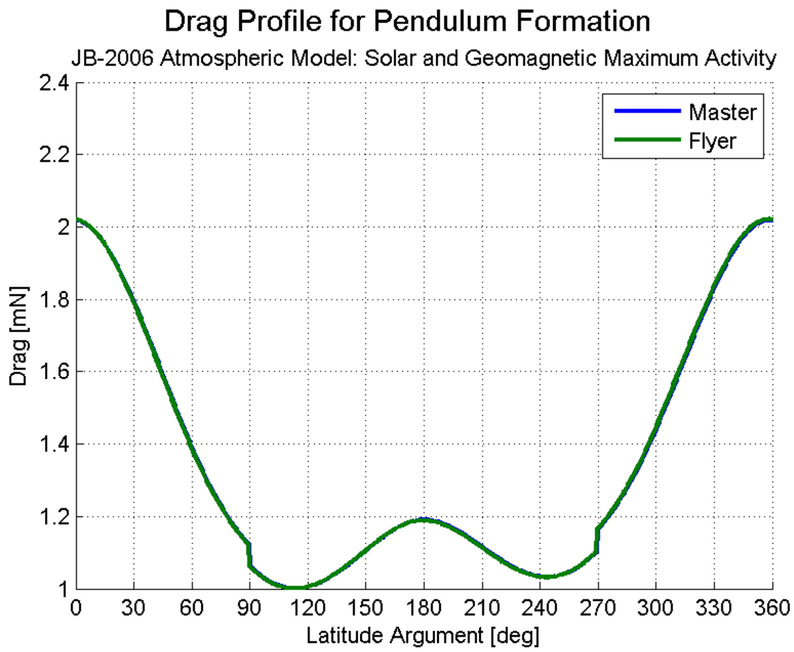

Figure 28: Differential Drag for Pendulum Formation. Maximum Solar and Geomagnetic Activity

3.3.3.2. Results for Mean Solar and Geomagnetic Activity

Pendulum drag profile over one orbit with the mean solar and geomagnetic activity corresponds to epoch B of Figure 21. As in the previous section, the differential drag is barely noticeable, since the only difference between the orbits is the RAAN or the inclination.

The second atmospheric scenario yields a range of variation along the complete orbit of [0.06 – 0.17] mN (Figure 29), with a maximum differential drag about 0.001 mN.

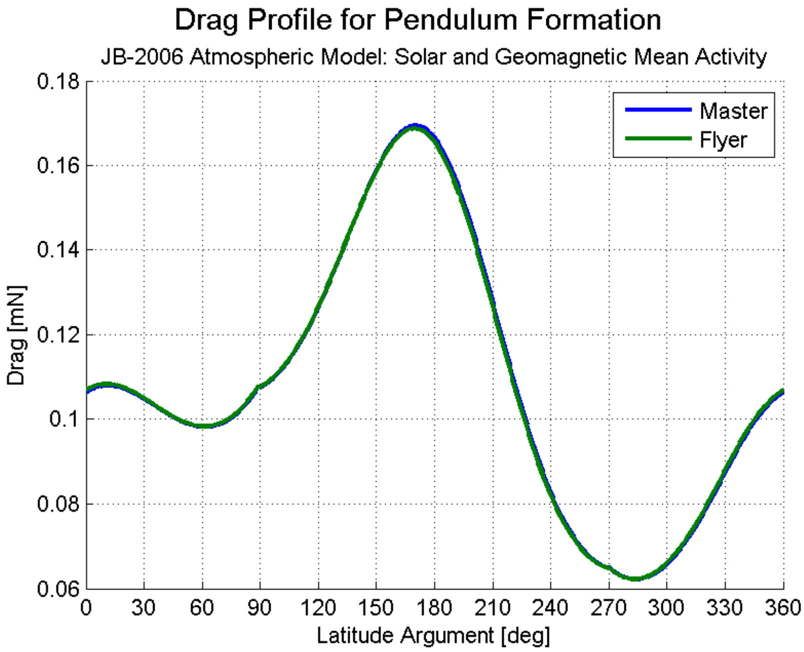

Figure 29: Differential Drag for Pendulum Formation. Mean Solar and Geomagnetic Activity

3.3.4. Cartwheel

In a **Cartwheel formation** the S/Cs revolve around each other. This FF topology can be obtained by applying the following deltas in Keplerian elements with respect to the reference orbit of the formation ([R.D.3]):

- Delta in eccentricity & argument of perigee (i.e., eccentricity vector) and mean anomaly.
- The satellites are located in the same orbital plane, i.e. no delta in inclination and RAAN are applied.

Figure 30 displays a Cartwheel formation for the NGGM with perigee/apogee separation of the two polar orbits along the north-south direction, corresponding to a 180º shift in the argument of perigee. The mean altitude of the two orbits is 350 km and their eccentricity is selected to achieve a mean satellite-to-satellite distance (d) of 75 km. This is obtained choosing a semi-major axis for both orbits of 6728 km and a nominal eccentricity of both orbits $e = 3.716 \cdot 10^{-3}$.

Though a Cartwheel can be obtained for any selected delta of the argument of perigee, in this case the delta is fixed to 180º, thus minimizing the necessary eccentricity and keeping the orbits almost circular.

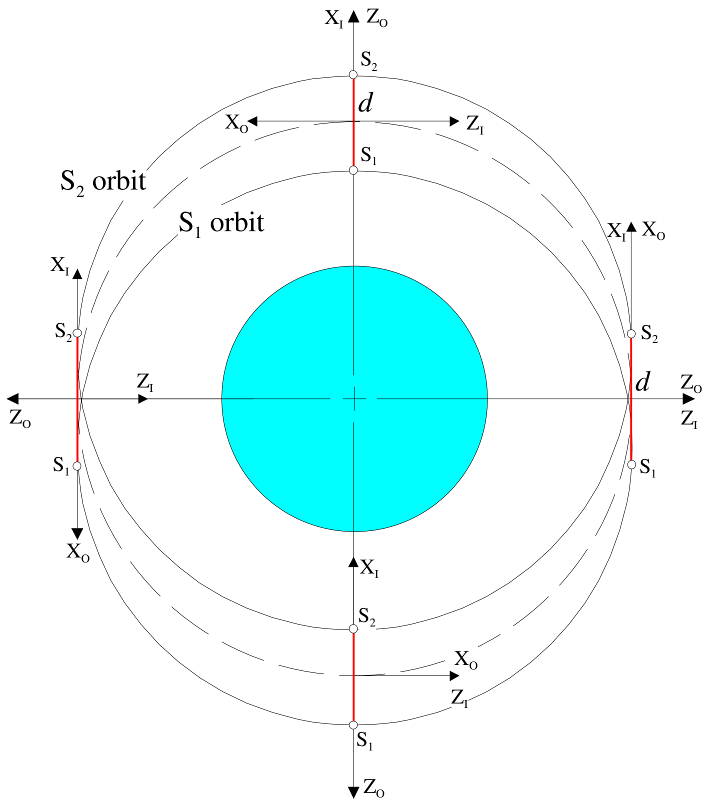

Figure 30: Cartwheel Formation Geometry for NGGM

Two configurations have been studied: one that achieves a vertical baseline over the equator and the other over the poles. The first case is the worst FF configuration. The maximum vertical separation is reached over the equator, where the altitude is lower due to the Earth flattening. This implies higher drag levels and a higher gradient that causes greater differential drag.

The second configuration is the opposite case, where the maximum vertical separation occurs in the most favourable position, since at the poles the altitude is at its highest point. Therefore the differential drag is lower.

The first configuration is analysed considering the worst epoch (highest density) within the solar cycle and the maximum solar and geomagnetic activity, while the second configuration is studied for the best epoch (lowest density) and the minimum solar and geomagnetic activity. Thus the results provide the range of differential drag that might appear, depending on both atmospheric activity and cartwheel FF design. There are other two relevant scenarios: best configuration with worst atmospheric activity and worst configuration with best atmospheric activity; however they would lead to intermediate results within that range, and therefore they have not been analysed.

3.3.4.1. Results for Maximum Solar and Geomagnetic Activity

Cartwheel drag profile over one orbit with the maximum solar and geomagnetic activity corresponds to epoch A of Figure 21. For this scenario, the Cartwheel formation considered is the one in which the spacecrafts have a vertical baseline over the equator. The keplerian elements of both S/Cs have different values for the argument of the perigee and the mean anomaly; for the first spacecraft the argument of the perigee is w = 90º and the mean anomaly is M = 270º, for the second w = 270º and M = 90º.

The results yield a range of variation along the complete orbit of [0.8 – 2.9] mN (Figure 31), while the maximum differential drag is about 1.4 mN. The variation of the eccentricity vector leads to altitude differences that cause a greater differential drag than in pendulum or in-line FF configurations.

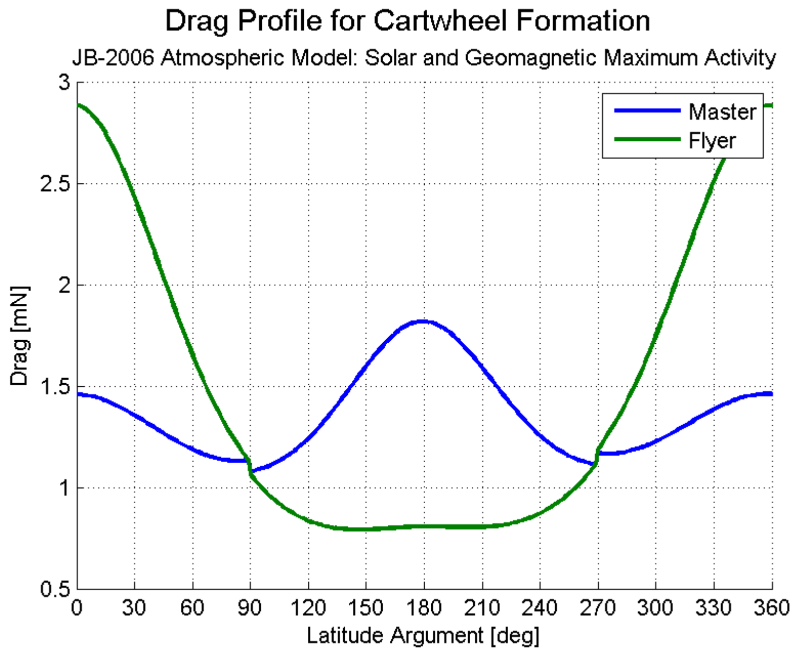

Figure 31: Differential Drag for Cartwheel Formation. Maximum Solar and Geomagnetic Activity

The differential drag at the ascending node crossing is different from the one obtained at the descending node crossing. This effect is due to the difference in local time for the ascending and descending nodes, as it is explained in section 3.2.

3.3.4.2. Results for Mean Solar and Geomagnetic Activity

Pendulum drag profile over one orbit with the mean solar and geomagnetic activity corresponds to epoch B of Figure 21. For this scenario, the Cartwheel formation considered is the one in which the spacecrafts have a vertical baseline over the poles. The keplerian elements of the S/Cs differ in the argument of the perigee and in the mean anomaly. For the first spacecraft the argument of the perigee is w = 0º and the mean anomaly is M = 0º, for the second one, w = 180º and M = 180º.

The results yield a range of variation along the complete orbit of [0.7 – 2.2] mN (Figure 31), while the maximum differential drag is about 0.8 mN. The variation of the eccentricity vector leads to altitude differences that cause a greater differential drag than in pendulum or in-line FF configurations.

.

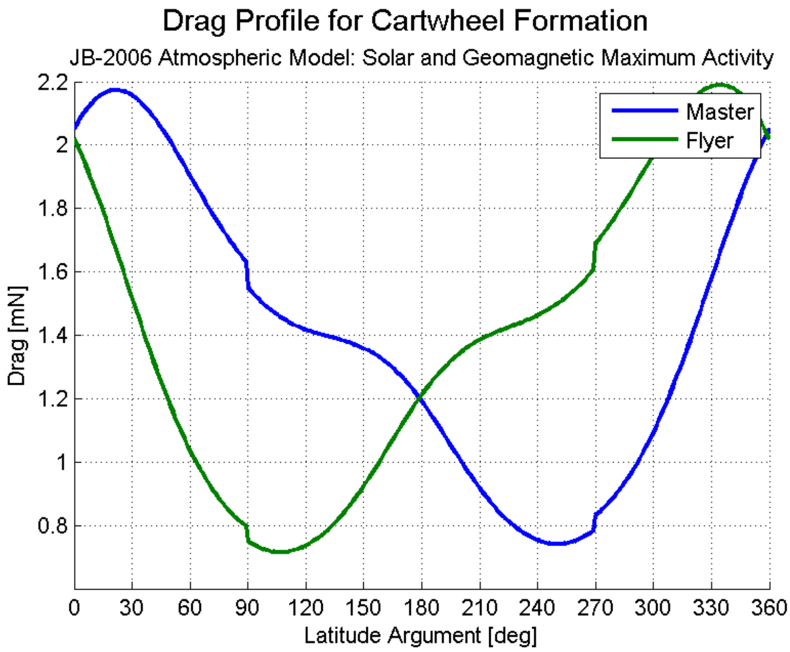

Figure 32: Differential Drag for Cartwheel Formation. Mean Solar and Geomagnetic Activity

3.3.5. Conclusion

In-line and Pendulum FF configurations provide the same results, with a narrower range of drag in each solar and geomagnetic case than with the Cartwheel. Besides, the maximum differential drag obtained for the former cases is almost negligible, while for the Cartwheel the differential drag is of the same order of magnitude as the range. All these results can be seen in Table 5.

	In-line	Pendulum	Cartwheel
Maximum solar and geomagnetic activity			
Minimum Drag [mN]	1.0	1.0	0.8
Maximum Drag [mN]	2.1	2.1	2.9
Maximum differential drag [mN]	0.007	0.007	1.4
Average solar and geomagnetic activity			
Minimum Drag [mN]	0.06	0.06	0.7
Maximum Drag [mN]	0.17	0.17	2.2
Maximum differential drag [mN]	0.001	0.001	0.8

Table 5: Differential Drag Results Summary

3.4. Additional Contributors to Atmospheric Drag

As demonstrated in the previous sections, the altitude and the solar and geomagnetic activity are the main drivers of the drag that a satellite experiences and may need to counteract. Table 4 shows that both a 100-km altitude variation and an epoch change within the same solar cycle can result in drag variations of about one order of magnitude.

This section presents qualitative considerations identifying other parameters that have a second-order influence on the drag, which in some cases may not be negligible. In order to do so, the entire study is based on a single set of solar and geomagnetic indexes, thus filtering out the effects of their variability.

The main feature of the atmospheric density distribution is its exponential decrease with the increase of the altitude. Therefore, not only the reference altitude of the orbit has an influence on the drag, but also its altitude profile, i.e. its eccentricity. Figure 33 shows on its left panel the altitude variation as a function of the latitude for a circular orbit (eccentricity close to zero) and for a frozen orbit. Both are polar orbits and have the same 250-km reference altitude. The frozen orbit is often chosen as it offers natural stability of the eccentricity vector, thus maintaining its altitude-vs.-latitude profile over long periods without any eccentricity control. It features a small eccentricity (~10^{-3}) and its perigee is located above the North Pole.

The right panel of Figure 33 shows the corresponding density profiles encountered by the satellite during one orbit. The X-axis is not the latitude but the time after ANX, going from zero to 1 orbital period. It is interesting to notice that, even in the case of the perfectly circular orbit (green curve), the Earth flattening introduces a factor 1.5 between the maximum and minimum densities experienced by the spacecraft. The asymmetry between the Poles introduced by the frozen altitude profile (blue curves) increases this difference up to a factor 1.9.

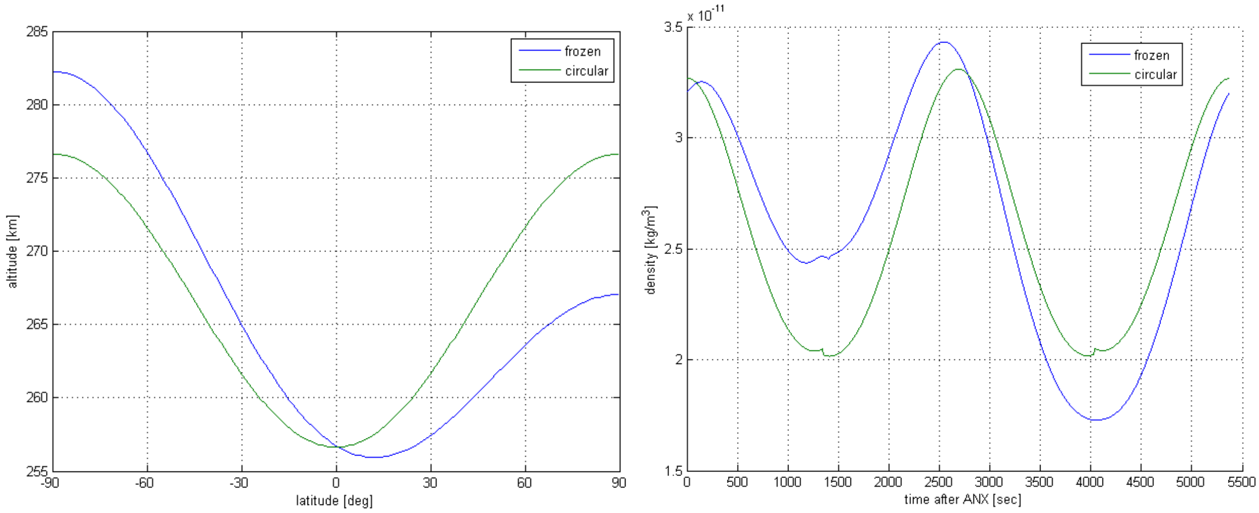

Figure 33: Altitude (left) and Density (right) Profiles of a Frozen (blue) and a Circular (green) Orbits

The second most important feature of the atmospheric density distribution is related to the daily Sun illumination. Figure 34 shows two snapshots of the atmospheric density at a constant altitude of 500 km, at summer solstice (left panel) and at winter solstice (right panel). The direct geometrical relationship between the Sun direction (orange arrow) and the density distribution is clearly visible.

One first conclusion is that low inclination orbits will always feature bumpy drag profiles.

The second conclusion is that for near-polar orbits, one key parameter is the local time at ascending node (LTAN).

Finally, the season may also play a role, depending on the orbital configuration. However, as this is linked to the date, it may probably be negligible with respect to the effects of the solar and geomagnetic activity.

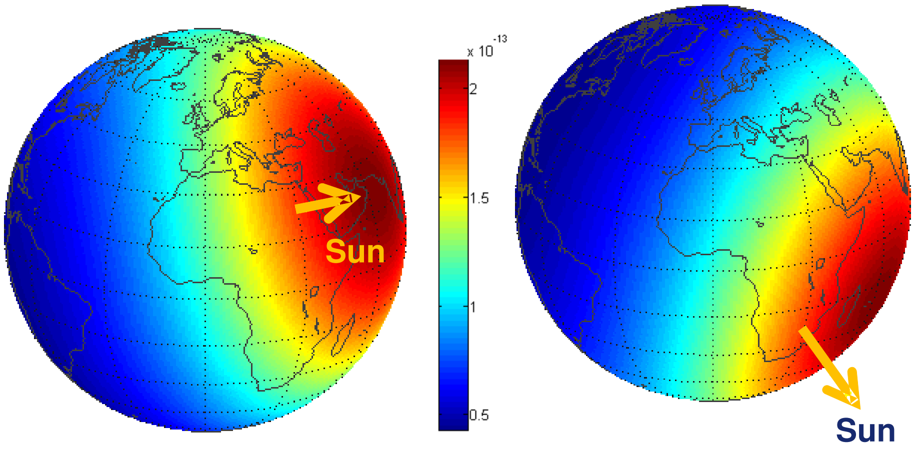

Figure 34: Atmospheric Density (kg/m^3) at 500 km, June 21st (left), December 21st (right)

Figure 35 shows more in detail the relationship between the LTAN and the drag for near-polar orbits. The left panel shows the density distribution at 250 km, seen from the North Pole, as well as the Sun direction and two orbits featuring LTANs offering opposite density profiles. The curves of the right panel show the real density profiles during one orbit, for 250-km polar circular orbits.

The green orbit, at 08:00, offers the smoothest drag profile. The blue one, at 14:00, features minimum and maximum density values separated by a factor 2.3. For both profiles, an important contributor of the density variation is the altitude variation due to the Earth flattening, which is not visible on the density map of the left panel (constant altitude).

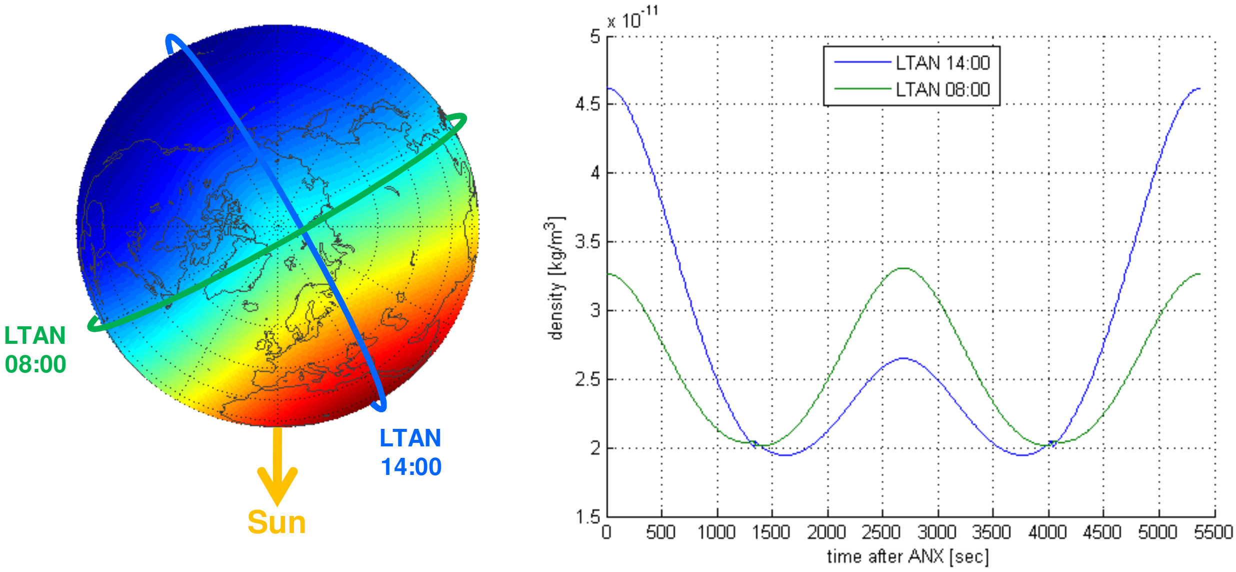

Figure 35: Influence of LTAN on Drag Profile for Near-Polar Orbits

Figure 36 illustrates the very small difference between the density profiles experienced from an SSO and a polar orbit, at 250 km and LTAN=08:00. A polar orbit will see its LTAN circle around the clock in one year, i.e. it will experience all the density profiles existing between the extreme ones shown on Figure 35. On the other hand, an SSO has a constant LTAN; it will therefore feature a constant drag profile as well.

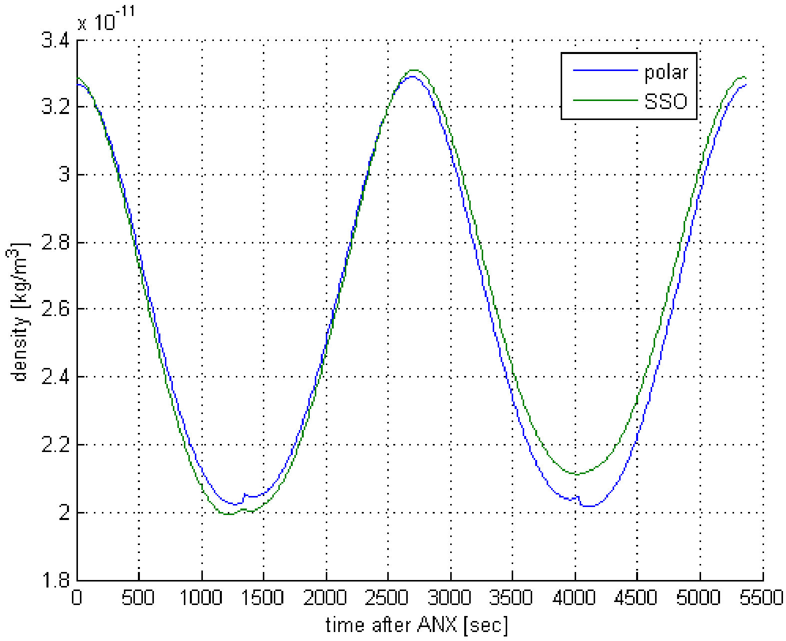

Figure 36: Density Profile of 250-km Orbits, LTAN 08:00, SSO and Polar

To conclude, if the reduction of the drag profile oscillation within one orbit is important, two main orbital parameters can be tuned:

- The **eccentricity** may be reduced as much as possible in order to minimize the strong influence of the altitude variation
- The orbit may be **Sun-synchronous**, with a **LTAN** of **08:00** (or 20:00) in order to minimize the effect of the day/night alternation on the atmosphere where the satellite flies.

4. FORMATION FLYING STABILITY ANALYSIS

4.1. Approach

The considered NGGM Formation Flying (FF) system comprises **two satellites** flying in different orbital configurations with a **baseline** (inter-satellite distance) of **75 km**.

The design and analysis rationale for FF missions encompasses mission analysis issues (for orbital and formation topology design) and Guidance, Navigation and Control (GNC) design issues (for formation maintenance and effective control, in accordance with the mission requirements). Therefore, the overall analysis approach is conceived as an iterative process that implements the logic illustrated in Figure 37.

Generally speaking, the **FF analysis** aims at identifying and estimating the most relevant effects of the orbital perturbations acting on the S/C, in order to define performance and cost implications. Such an analysis shall focus both on the absolute perturbations affecting the motion of each S/C considered as a stand-alone mission, and on the effect of differential perturbations due to differential position and/or S/C mass and layout, leading to a degradation of the formation.

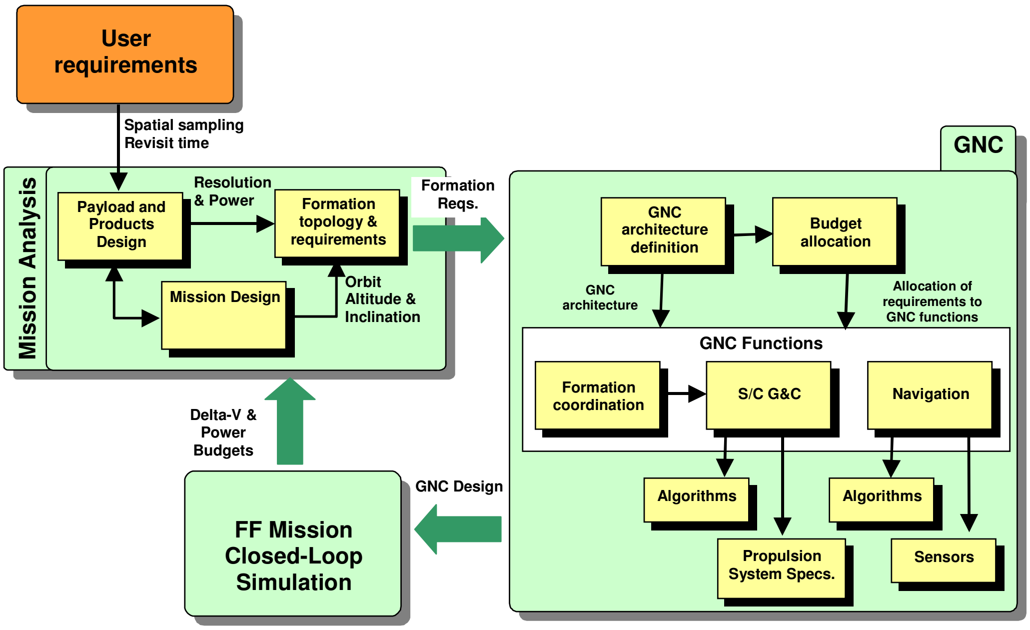

Figure 37: Analysis Approach for FF-Based Missions

The key outputs of the FF orbital analysis are:

- Identification and assessment of the perturbation effects that are relevant for the given formation-flying mission.
- Estimation of the evolution of the satellite orbits (relevant for orbit control) and of the relative position and velocities of the S/C, one with respect to the other (relevant for formation maintenance).
- Identification of typical orbit correction and formation maintenance manoeuvres aimed at the estimation of ΔV and propellant budgets and the evaluation of the impact on the mission operations.

On the other hand, and also in a generic way, it can be said that the **FF design** provides the initial relative satellite geometry to achieve the required inter-satellite baseline. The relative orbital evolution of the two satellites is driven by the relative perturbation effects that most noticeably degrade the designed relative configuration.

In the case of a formation mission in LEO like NGGM, the major effects to be taken into account (either to counteract them or to be considered as part of the mission outcomes) are the following:

- **Effect of differential drag perturbations**. Drag forces degrade the relative motion if a difference in the ballistic coefficients of the two S/C exists (for any atmospheric drag or Solar Radiation Pressure coefficients). In the case of atmospheric drag, the induced acceleration is always directed parallel, and in the opposite direction, with respect to the flight velocity. The direct consequence is that satellites having different ballistic coefficients are characterised by different decay velocities, which translates into differences in orbital periods, leading to a relative longitudinal motion.
- For the **Solar Radiation Pressure**, the prediction of the relative motion behaviour is in general more complex than in the atmospheric drag case, since the orientation of the relative acceleration largely changes along the mission lifetime in the local reference frame. If the reference orbit is Sun-Synchronous, it is expected that the relative acceleration is on average directed along a certain privileged direction and, hence, that an estimation of this effect could be thoroughly assessed.
- **Effect of gravitational perturbations**. Forces due to the non-spherical components of the Earth gravitational potential also cause degradation in the natural geometry, which must be accounted as specified by mission requirements. For in-track formations this effect is minimised since the satellites are supposed to fly the 'same orbit' and follow the same ground track, i.e., they pass over the same points of the Earth but at slightly different times. However, since this in-track topology cannot be exactly achieved for all latitude ranges with natural orbits, the effect induced by the potential harmonics (not only zonal ones, but also tesseral ones) leads in general to a secular, non-periodic relative motion. In this case, the gravitational effect is mostly observed in the short-time scale (typically, one orbit and similar periods), since secular drifts are attenuated by the in-track condition.

The effects of the atmospheric drag have been analysed in section 3 to provide the inputs needed to define the propulsion system that guarantees its compensation.

As the NGGM could implement drag-free orbit control, the stability analysis of the possible FF configurations shall be carried out assuming that the satellites are flying in drag-free conditions and that the relevant perturbations to be considered are the gravitational perturbations. These perturbations trigger a differential relative motion of the two satellites with respect to the initial formation design corresponding to the reference baseline. Hence, a formation control strategy should be envisaged if the relative S/C baseline did no longer fulfil the required boundaries after a given time interval.

An **open-loop analysis** shall be performed to assess the medium and long-term evolution of the baseline without FF control, accounting at least for gravitational perturbations, so as to determine whether the baseline becomes incompliant with the associated bounds. Ultimately, the **analysis of the formation stability** with respect to the orbital perturbations is intended to assess whether the degradation of the relative satellite geometry prompts a dedicated FF closed-loop control strategy.

In this phase of the mission study the formation initialisation errors have not been taken into account, assuming a perfect initialisation. Otherwise, initial position and velocity dispersions may affect the formation degradation, having a driving impact in some cases ([R.D.3] and [R.D.4]).

The same formation configurations as for the drag analysis shall be considered:

- In-line (in-plane) formation.
- Cartwheel formation.
- Pendulum formation.

Each configuration is studied including 3 different sets of perturbations following an incremental strategy, in order to evaluate the contribution of each perturbation. They include:

- The Earth gravity field up to order and degree 30x30
- The Earth gravity field up to order and degree 30x30, plus the Sun and Moon gravity
- The Earth gravity field up to order and degree 30x30, plus the Sun and Moon gravity, plus a differential acceleration of 10^{-7} m/s^2 (simulating a bias between the drag-free thrusters of the satellites)

The results provide information on the amplitude and period of the perturbations that the spacecrafts have to cope with, supporting a trade-off analysis of the configurations.

4.2. In-line Formation

4.2.1. Earth Gravity Perturbation Effects

The time evolution of the baseline is assumed as an indicator of the long-term formation stability. The following Figure 38 shows the mid-term relative evolution (1-month period) of an in-line formation with a 75-km initial baseline. The only dynamic effect considered is the one stemming from Earth gravitational perturbations (gravity field up to order and degree 30x30).

As it can be seen, this configuration is basically stable under the effects of just Earth gravitational perturbations in a time range of 1 month, with a variation with respect to the nominal baseline of about 0.2 km. Nevertheless, the baseline degradation is increasing with time with a tendency that seems to lead to a complete divergence for long-term evolution of the formation. Therefore a longer simulation was run accounting for 1 year, with the results shown in Figure 39. The baseline is not indefinitely increasing, but oscillating, with a very small secular increase with time, confirming the stability of this configuration.

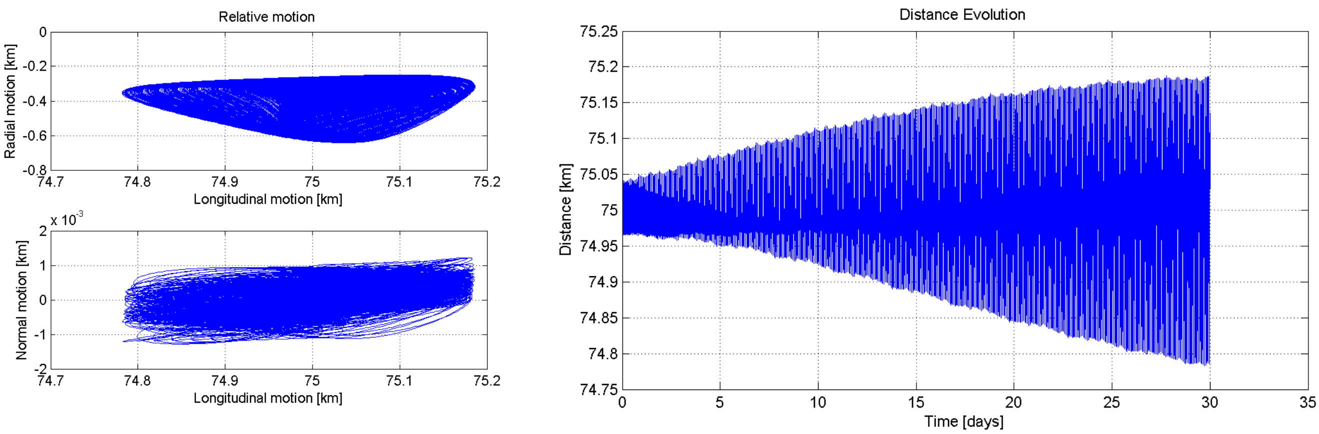

Figure 38: In-Line Formation Stability Analysis - Earth Gravity

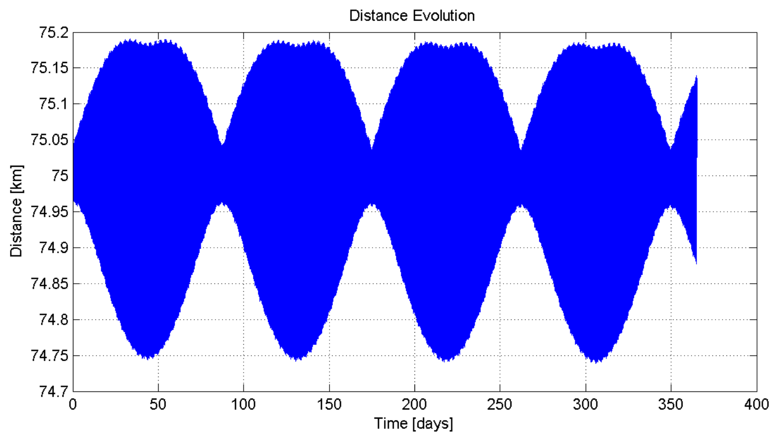

Figure 39: In-Line Formation Stability Analysis - Earth Gravity (1 year)

4.2.2. Total Gravity Perturbation Effects

The following Figure 40 shows the mid-term relative evolution (1-month period) considering the dynamic effects stemming from total gravitational perturbations:

- Earth gravity field up to order and degree 30x30
- Sun gravity
- Moon gravity

This configuration is also basically stable under the effects of just total gravitational perturbations in a time range of 1 month, with a variation with respect to the nominal baseline of about 0.2 km. As it happened under the effects of only Earth gravity, the baseline degradation is increasing with time with a tendency that seems to lead to a complete divergence for long-term evolution of the formation. Therefore a longer simulation was run accounting for 1 year, with the results shown in Figure 41. The baseline is not indefinitely increasing, but oscillating and with a small secular increase with time, although bigger than in Figure 39. Nevertheless it confirms the stability of this configuration.

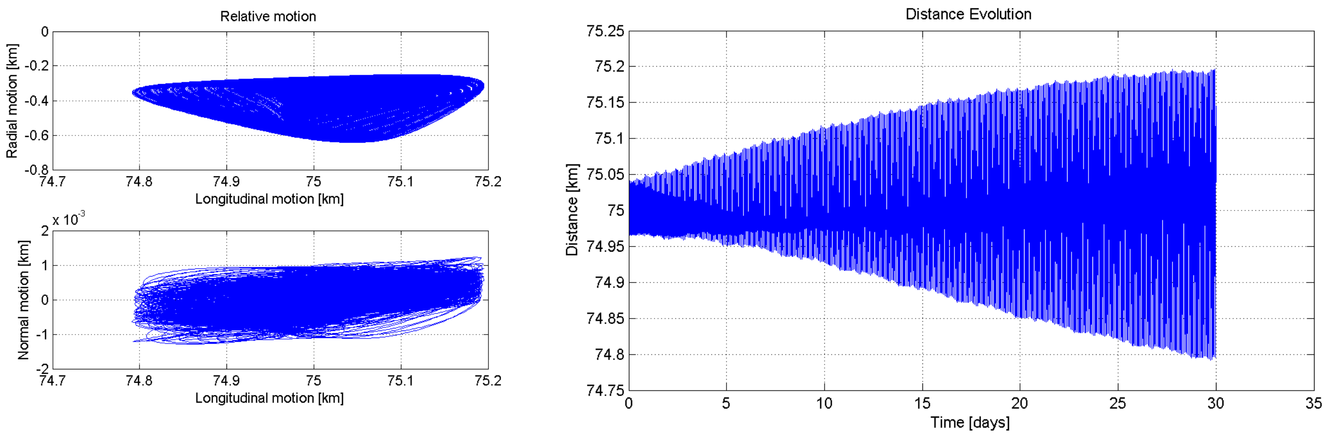

Figure 40: In-Line Formation Stability Analysis - Total Gravity

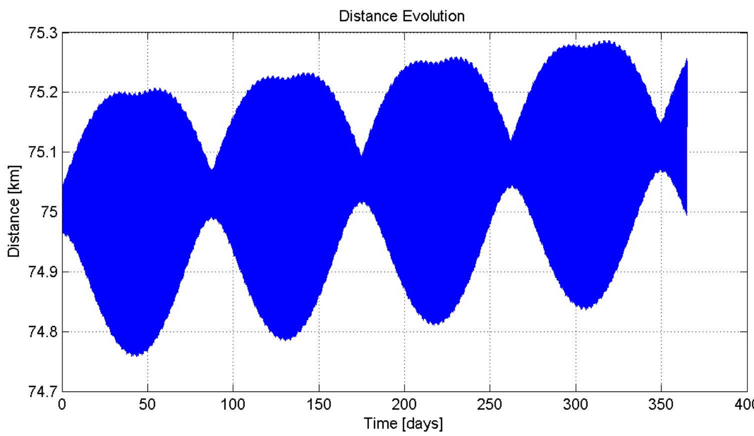

Figure 41: In-Line Formation Stability Analysis - Total Gravity (1 year)

4.2.3. Total Gravity Perturbation + Differential Thrust Bias Effects

The following Figure 42 shows the mid-term relative evolution (1-month) considering the dynamic effects stemming from total gravitational perturbations and a differential thrust bias of ± 10^{-7}m/s^2.

The effects introduced by the differential thrust destabilise the formation, leading to distances over 1000 km after a month. The sign of that bias, i.e. whether it brings the S/Cs closer or further, shall be taken into account. In one case the inter-satellite distance diminishes to zero (blue curves), while in the other the distance continuously increases (green curves).

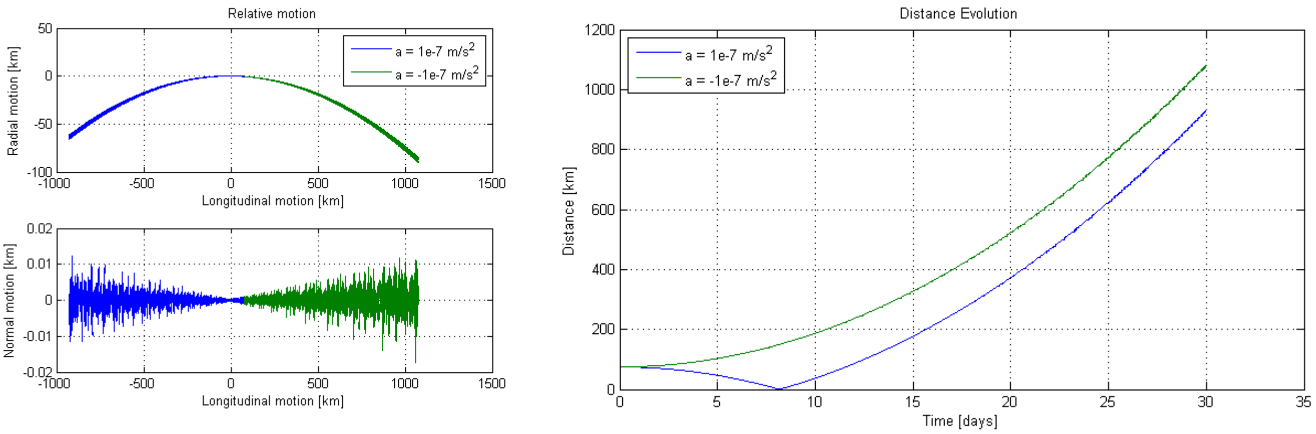

Figure 42: In-Line Formation Stability Analysis - Total gravity + Differential Thrust Bias

4.3. Pendulum Formation

Pendulum formation can be obtained by means of delta in RAAN and/or inclination. Since the results regarding formation stability are substantially different, they are presented separately. Section 4.3.1, describes the evolution with time of the formation defined by a delta in inclination with different perturbations, while section 4.3.2 provides the stability results in the case of using a delta in RAAN for formation design.

The time evolution of the baseline is assumed as an indicator of the long-term formation stability.

4.3.1. Pendulum with Delta in Inclination

4.3.1.1. Earth Gravity Perturbation Effects

The following Figure 43 shows the mid-term relative evolution (1-month period) of a pendulum formation with a 75-km initial baseline. The only dynamic effect considered is the one stemming from Earth gravitational perturbations (gravity field up to order and degree 30x30).

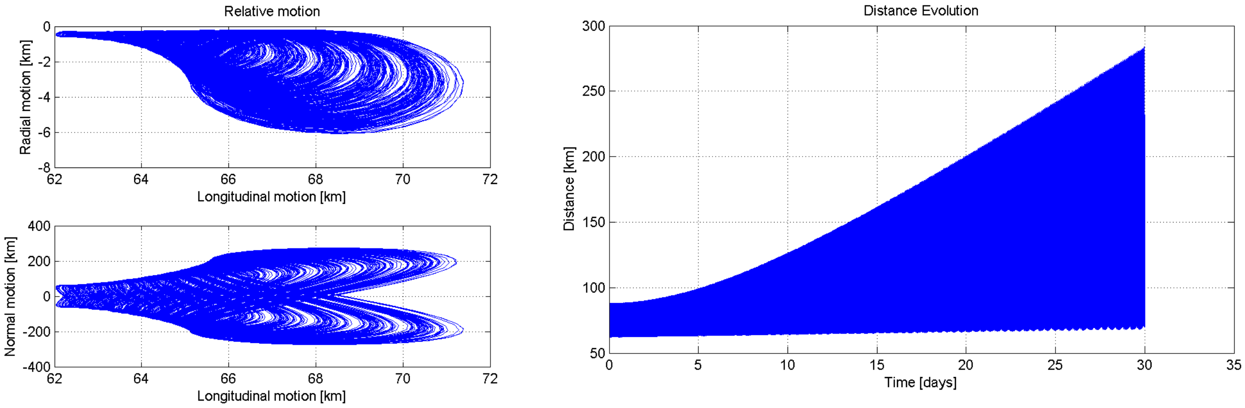

Figure 43: Pendulum Formation (Delta in Inclination) Stability Analysis - Earth Gravity

The natural drift in the presence of just gravitational forces (see Figure 44) is clearly shown in the open-loop distance evolution of the formation over one month presented in Figure 43. It leads to a deviation of the baseline distance of 200 km after one month

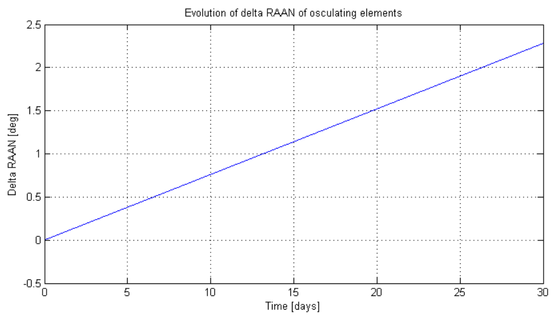

Figure 44: Differential Nodal Drift for Pendulum Formation with Delta in Inclination

4.3.1.2. Total Gravity Perturbation Effects

The following Figure 45 shows the mid-term relative evolution (1-month period) considering the dynamic effects stemming from total gravitational perturbations:

- Earth gravity field up to order and degree 30x30
- Sun gravity
- Moon gravity

The results are basically the same as obtained with only Earth Gravity. After one month the maximum baseline increases by 200 km.

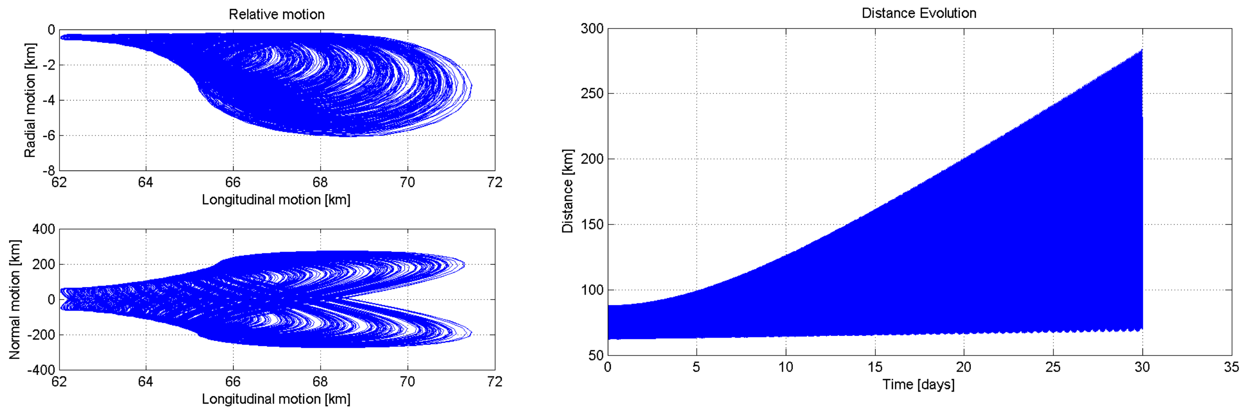

Figure 45: Pendulum Formation (Delta in Inclination) Stability Analysis - Total Gravity

4.3.1.3. Total Gravity + Differential Thrust Bias Effects

Considering the dynamic effects stemming from total gravitational perturbations and a differential thrust bias of ± 10^{-7}m/s^2, the stability of the formation is no longer fulfilled. The formation is led to an unstable situation where the inter-satellite distance reaches values over 1000 km, like in the in-line formation case. The sign of the differential thrust shall be considered, since the effects on total distance are different; see Figure 46.

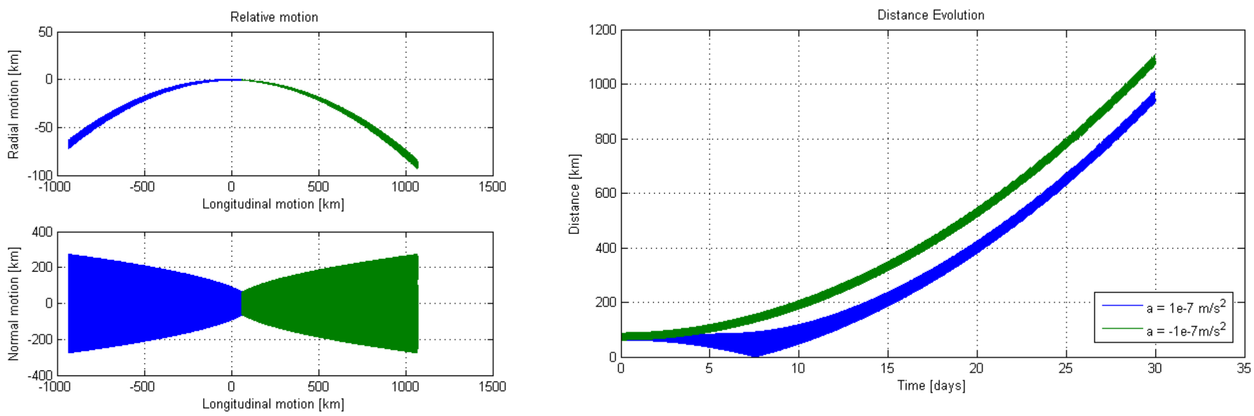

Figure 46: Pendulum Formation (Delta in Inclination) Stability Analysis - Total Gravity + Differential Thrust Bias

4.3.2. Pendulum with Delta in RAAN

4.3.2.1. Earth Gravity Perturbation Effects

The relative evolution shown in Figure 47 corresponds to effects stemming from Earth gravity perturbations. The design imposes a deviation with respect to the baseline distance (75 km) of ± 13km, while the gravity adds to the design deviations of only 0.3 km after one month.

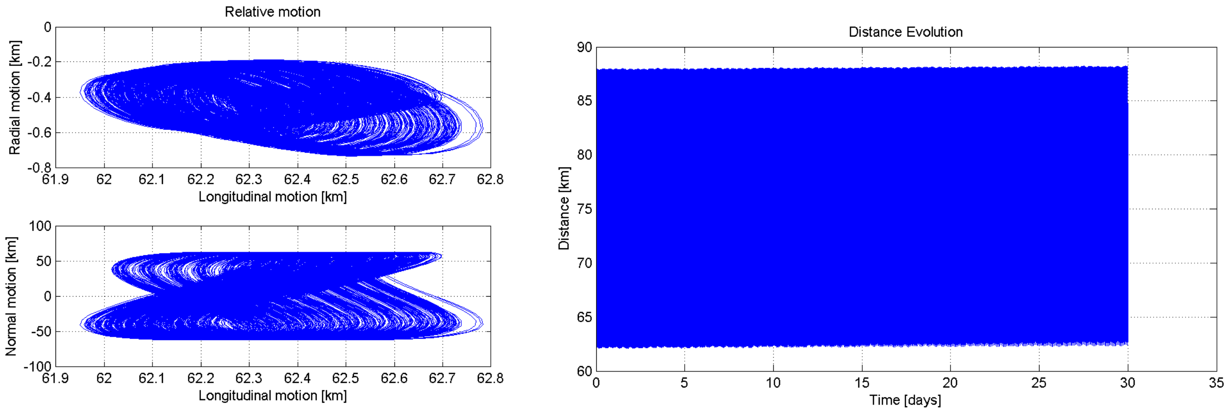

Figure 47: Pendulum Formation (Delta in RAAN) Stability Analysis – Earth Gravity

4.3.2.2. Total Gravity Perturbation Effects

Figure 48 shows the 1-month period relative evolution considering the dynamic effects stemming from total gravitational perturbations:

- Earth gravity field up to order and degree 30x30
- Sun gravity
- Moon gravity

Sun and Moon effects do not change substantially the stability. The deviation with respect to design maximum distance is approximately the same as obtained with only the Earth gravity deviation: 0.3 km.

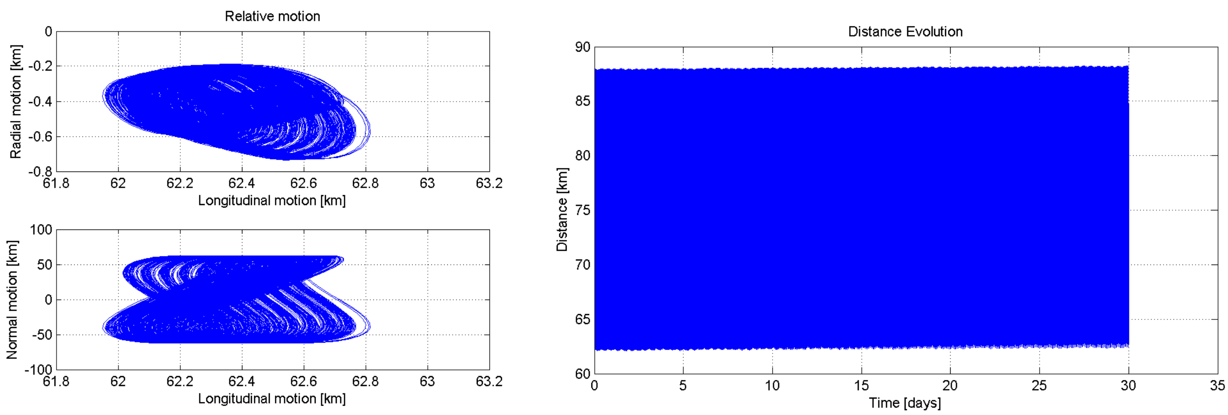

Figure 48: Pendulum Formation (Delta in RAAN) Stability Analysis - Total Gravity

4.3.2.3. Total Gravity + Differential Thrust Bias Effects

The addition of a differential thrust bias causes similar effects as for in-line formation or for Pendulum with delta in inclination. A large divergence in the longitudinal motion leads to an inter-satellite distance over 1000 km in one month.

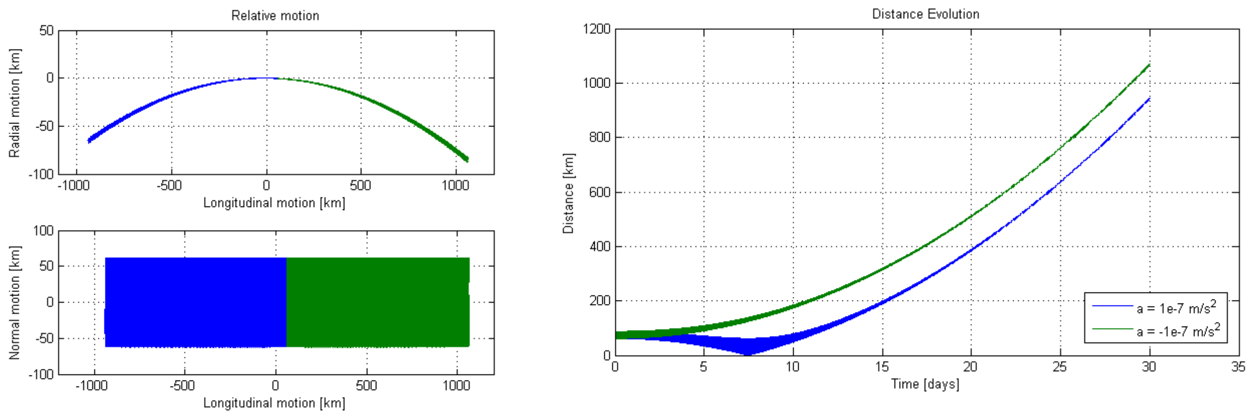

Figure 49: Pendulum Formation (Delta in RAAN) Stability Analysis - Total Gravity + Differential Thruster Bias

4.4. Cartwheel Formation

The Cartwheel formation has been designed with two different solutions: one with satellite vertical alignment over the poles and the other over the equator. Assuming drag-free conditions, the effects on formation stability are practically the same, with equal deviations with respect to the nominal inter-satellite distance. Therefore, only the influence of different perturbation effects is considered in the following paragraphs.

4.4.1. Earth Gravity Perturbation Effects

Figure 50 contains the results of the FF stability for Earth gravity. The FF design leads to variations on the distance between 50 and 100 km. Besides this variation, the gravity introduces an additional deviation of 5 km, for a 1-month simulation.

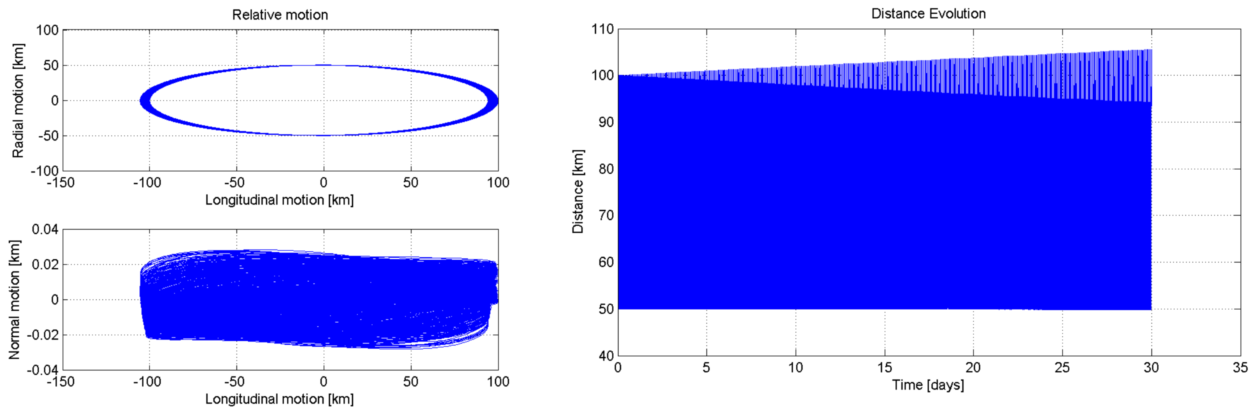

Figure 50: Cartwheel Formation Stability Analysis - Earth Gravity

4.4.2. Total Gravity Perturbation Effects

The results obtained for total gravity effects corroborates the small effect of Sun and Moon gravity on the FF stability, as it happens with in-line and pendulum formations. The deviation with respect to design maximum distances is also 5 km as in the case of only Earth gravity.

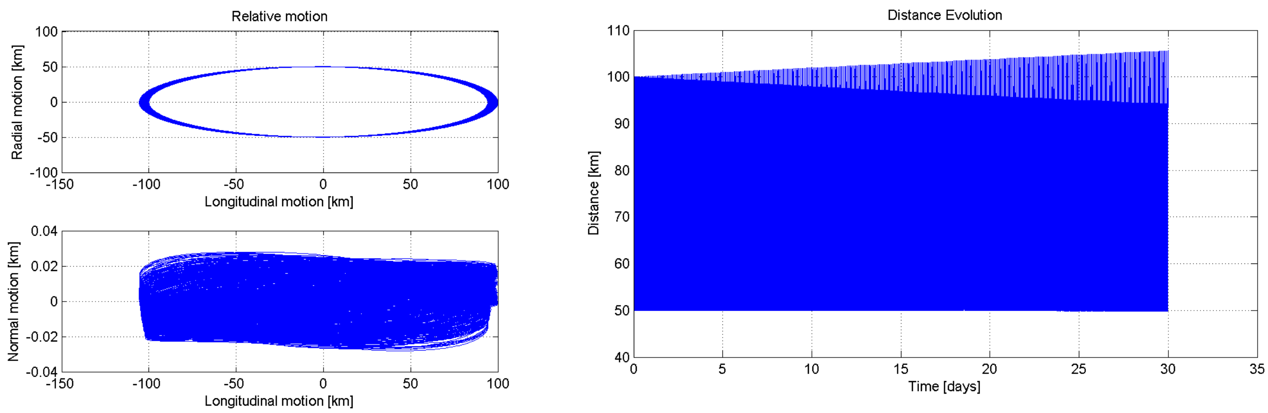

Figure 51: Cartwheel Formation Stability Analysis - Total Gravity

4.4.3. Total Gravity Perturbation + Differential Thrust Bias Effects

Finally, the differential thrust bias causes the largest effects, destabilising the formation, as it is shown in the open loop evolution over 1 month exposed in Figure 52.

The inter-satellite distance increases its variation margin, reaching a minimum distance of zero, in the lower boundary and increasing up to 1000 km for the upper limit.

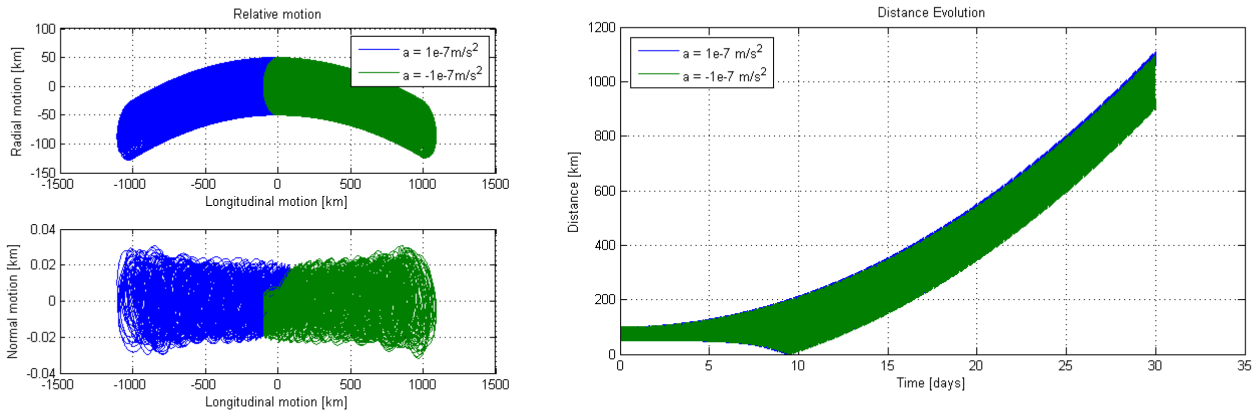

Figure 52: Cartwheel Formation Stability Analysis – Total Gravity + Differential Thrust Bias

4.5. Conclusion

The results obtained with all the FF configurations lead to two main conclusions regarding the perturbations considered for each case. First, the effects of Sun and Moon gravity are overshadowed by Earth gravity since the orbit altitude of the analyses is only 350 km. Increasing the orbit altitude might increase as well the relevance of Sun and Moon effects. The second conclusion is that the differential thrust bias has a driving impact on any configuration stability, decreasing the minimum baseline to zero, or increasing it to more than 1000 km in one month.

The comparison of the configurations brings to the fore that the most stable configuration is the in-line FF. Nevertheless, though the resulting motion of Pendulum FF with delta in RAAN is not as stable as the one obtained for the in-line, it is much less unstable than the Pendulum with deltas in inclination. The delta in inclination needed to obtain an inter-satellite distance of 75 km leads to an important differential RAAN drift that destabilises the formation in a very short time.

The deviation of the Cartwheel with respect to the nominal configuration is small (5 km), but it shall be taken into account that the design implies an oscillation of the baseline of ±25 km, bigger than for the Pendulum (±13 km).

All the results are summarised in Table 6, with approximate distance values.

	Design distance w.r.t 75 km	Maximum deviation w.r.t design
In-plane		
Earth Gravity	-	0.2
Total Gravity	-	0.2
Total Gravity + Differential thrust bias	-	1000
Pendulum – delta inclination		
Earth Gravity	± 13	200
Total Gravity	± 13	200
Total Gravity + Differential thrust bias	± 13	1000
Pendulum – delta RAAN		
Earth Gravity	± 13	0.3
Total Gravity	± 13	0.3
Total Gravity + Differential thrust bias	± 13	1000
Cartwheel		
Earth Gravity	± 25	5
Total Gravity	± 25	5
Total Gravity + Differential thrust bias	± 25	1000

Table 6: FF Stability Summary

However, besides the stability of the formations, other parameters related to scientific requirements shall be considered to select the most appropriate configuration.

END OF THE DOCUMENT